

Infrared finiteness in the factorization of the dijet cross section in hadron-hadron collision near threshold

Junegone Chay,^{1,*} Taewook Ha,^{1,†} and Inchol Kim^{1,‡}

¹*Department of Physics, Korea University, Seoul 136-713, Korea*

Abstract

The factorization theorem for the dijet cross section is considered in hadron-hadron collisions near threshold with a cone-type jet algorithm. We focus on the infrared finiteness of the factorized parts by carefully distinguishing the ultraviolet and infrared divergences in dimensional regularization. The soft function, subject to a jet algorithm, shows a complicated divergence structure. It is shown that the soft function becomes infrared finite only after the emission in the beam directions is included. Among many partonic processes, we take $q\bar{q} \rightarrow gg$ as a specific example to consider the dijet cross section, and verify explicitly that each factorized part is infrared finite. We also compute the anomalous dimensions of the factorized components to next-to-leading logarithmic accuracy. The hard and the soft functions have nontrivial color structure, while the jet and the collinear distribution functions are diagonal in color space. The dependence of the soft anomalous dimension on the jet algorithm is color diagonal and is cancelled by that of the jet functions. The sum of the remaining anomalous dimensions also cancels, thus the dijet cross section is independent of the renormalization scale.

arXiv:1607.08010v1 [hep-ph] 27 Jul 2016

* E-mail:chay@korea.ac.kr

† E-mail:hahah@korea.ac.kr

‡ E-mail:vorfeed@korea.ac.kr

I. INTRODUCTION

The study of jet physics in high energy scattering has reached a sophisticated level. Many of the factorization theorems for inclusive scattering processes have been established both in QCD and in soft-collinear effective theory (SCET) [1–3]. More differential quantities such as the transverse momentum dependence of the final-state particles or jets [4], and the jet substructures [5] have been studied. Though we probe more differential quantities, not all the factorization theorems are provided yet. But the factorization theorems should be proved since they offer a fundamental basis for theoretical predictive power.

In general, the factorization theorem states that the prediction for physical observables consists of the product or the convolution of the hard, the collinear and the soft parts. In proving the factorization theorem for various scattering processes, it is important to verify that each factorized part is infrared (IR) finite. Otherwise the dependence of the renormalization scale does not solely come from the ultraviolet (UV) divergence, which invalidates the scaling behavior of the factorized parts. If some components are not IR finite in the factorized form, the factorized parts should be reshuffled such that the redefined or rearranged quantities are IR finite. If the IR divergence remains even after the rearrangement, the quantity at hand is not physical.

A fully inclusive quantity is IR finite to all orders due to the Kinoshita-Lee-Nauenberg theorem [6, 7] since the IR divergence from the virtual correction is cancelled by that of the real correction. It should hold true also for exclusive physical quantities such as the dijet cross section, in which the phase space for the real gluon emission is constrained by the jet algorithm.

The verification that each factorized part is IR finite in the dijet cross section from e^+e^- annihilation with various jet algorithms has been performed in Refs. [8, 9]. On the other hand, here we take the dijet cross section in hadron-hadron collision near threshold with a cone-type jet algorithm [10] to show explicitly that each factorized part is IR finite by carefully dissecting the phase space and performing the corresponding computation. This process is more complicated due to the complex color structure and the existence of the beam hadrons, thus more illuminating to show how to disentangle the interwoven structure of divergence.

The dijet cross section in hadron-hadron collision near threshold is shown to be factorized into the hard, collinear and soft parts, which is schematically written as

$$\sigma_J \sim \text{tr}(\mathbf{H} \otimes \mathbf{S}) \otimes f_{i/N_1} \otimes f_{j/N_2} \otimes \mathcal{J}_3 \otimes \mathcal{J}_4. \quad (1)$$

A more rigorous expression will be derived in Sec. II. Here \mathbf{H} is the hard function depending only on the hard scales, and \mathbf{S} is the soft function which describes the soft interactions among the energetic particles. The hard and soft functions are matrices in color space because they arise from different color channels. Near threshold, the incoming partons are described by the collinear distribution functions $f_{i/N}$, for the parton i to be contained in the hadron N , rather than the parton distribution functions (PDFs) $\phi_{i/N}$. The distinction will be discussed later. And \mathcal{J}_i are the integrated jet functions describing the outgoing collinear particles prescribed by a jet algorithm in the final state.

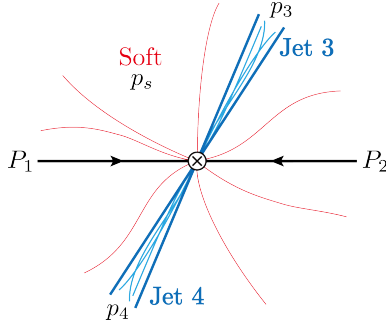


FIG. 1. A schematic diagram for the dijet production in hadron-hadron scattering near threshold. From the hadrons with momenta P_1 , and P_2 , the partons with the momenta p_1 and p_2 undergo a hard scattering. The two jets with their momenta p_3 and p_4 are produced. The soft momentum p_s is either inside or outside the jet depending on the jet algorithm.

The configuration of the dijet production near threshold is schematically shown in Fig. 1. The incoming partons with momenta p_1 and p_2 take most of the momenta from the two hadrons with momenta P_1 and P_2 and participate in the hard collision. Then the partonic CM frame coincides with the hadronic CM frame. Jet algorithms in e^+e^- annihilation and in hadron-hadron scattering are different since the latter should preserve the boost invariance along the beam direction. However, near threshold, we can employ the same cone-type jet algorithm with the rescaling of the jet radius [11]. For central jets with the rapidity close to zero, the cone-type jet algorithms in both cases take the same form.

Since the partons are back to back in the hadronic CM frame near threshold, the resultant dijets are also produced back to back. Away from the threshold, the dijets do not have to be back to back, and the initial-state particles also form beam jets in the beam direction. In this case, the factorized form for the jet cross section retains almost the same form except that the collinear distribution functions are replaced by the beam functions [12], describing the emission of the collinear particles along the initial parton from the hadron. This case will be investigated later, and here we consider the dijets near threshold.

In every high-energy process, the IR finiteness should be guaranteed, but here we focus on the dijet cross section to illustrate how carefully the UV and IR divergences should be treated. We examine various radiative corrections by carefully separating the UV and IR divergences and show that each factorized part is indeed IR finite. This type of analysis should be applied to other various differential processes for the rigorous proof of the factorization theorems.

The claim that the factorization of the cross section is established is to verify that each factorized part should be free of IR divergence. Numerous types of computations have been performed to extract the UV divergence either by applying the dimensional regularization or by introducing some IR regulators. In many cases, the divergences appearing in the computation are regarded as the UV divergence based on the belief that the factorized parts are physical quantities, hence should be free of IR divergence. However, the mere separation of the long- and short-distance effects via the factorization guarantees in no way that each factorized part is IR finite. It should be rather explicitly checked than presumed. If each

factorized part is IR free, the factorization theorem remains valid. If not, a new combination should be devised such that there is no IR divergence in the recombined parts. In fact, if the divergences are carefully distinguished, there may remain IR divergence, which endangers the validity of the factorization. This aspect will be investigated in detail here.

Only after the remaining divergence is guaranteed to be of the UV origin, we can safely apply the renormalization group equation to resum large logarithms. In this paper, we employ the pure dimensional regularization with the spacetime dimension $D = 4 - 2\epsilon$ and the $\overline{\text{MS}}$ scheme, in which we carefully distinguish the UV and the IR divergences in computing radiative corrections of the jet and soft functions with a jet algorithm. Especially in the soft function, there exist IR divergences if we naively apply the jet algorithm. However, we have found some additional contributions from the phase space pertaining to the beam directions. By including this contribution, the soft function becomes IR finite, and we have a firm status in proving the factorization theorem. It will be explained in detail in Sec. III.

The dijet cross section is described by $2 \rightarrow 2$ processes at the parton level. We can analyze all the processes, but we rather choose the specific process $q\bar{q} \rightarrow gg$ to show how the extraction of the IR divergence works. This process involves the computation of the gluon jet function with the jet algorithm, while the quark jet function with the jet algorithm was calculated in Ref. [8, 13, 14]. And the structure of the hard and soft functions is interesting and complicated enough to seek the consistency in the relations among the anomalous dimensions.

This paper is organized as follows: The factorization of the dijet cross section in hadron-hadron collision is presented in Sec. II. We take a specific example of the partonic process $q\bar{q} \rightarrow gg$ to express the individual factorized components explicitly. In Sec. III, we discuss the main ideas and techniques, in which we explain the structure of the phase space for the soft function and the technical details in dimensional regularization to handle the aforementioned phase space. In Sec. IV, the soft function is computed with the jet algorithm. The cancellation of the IR divergence is the most nontrivial issue and it will be treated in detail. In Sec. V, the gluon jet function and its anomalous dimensions are computed with the cone-type algorithm at next-to-leading order. In Sec. VI, the collinear distribution function, and its anomalous dimension are computed at one loop. In Sec. VII, we collect the anomalous dimensions of the hard, soft, jet and collinear distribution functions at one loop. The independence of the renormalization scale in the dijet cross section is confirmed explicitly. In Sec. VIII, the conclusion and the perspective are presented. In Appendix A, the detailed computation is presented for the real gluon emission in the soft part from the beam-jet contributions. In Appendix B, the soft contribution along the beam direction is derived both from the beam-beam and the beam-jet contributions.

II. FACTORIZATION OF THE DIJET CROSS SECTION

We consider the dijet cross section in hadron-hadron collisions near threshold

$$N_1(P_1) + N_2(P_2) \rightarrow j_3(p_3) + j_4(p_4) + X_s, \quad (2)$$

where N_1 and N_2 are incoming hadrons (protons in the case of LHC), j_3 and j_4 denote two back-to-back energetic collinear jets and X_s represents soft particles. Near threshold, the momenta of the incoming partons p_1 and p_2 are close to the hadronic momenta P_1 and P_2 respectively. We choose the beam directions to be in the n_1 and n_2 directions with $n_1^2 = n_2^2 = 0$, $n_1 \cdot n_2 = 2$, and $\bar{n}_1 = n_2$. The jet directions are chosen to be n_3 , and n_4 with $n_3^2 = n_4^2 = 0$, $n_3 \cdot n_4 = 2$, and $\bar{n}_3 = n_4$. And we consider the dijets away from the beam direction, which can be stated as $n_1 \cdot n_3 \sim n_1 \cdot n_4 \sim \mathcal{O}(1)$.

The dijet cross section near threshold in SCET is written as

$$\begin{aligned} \sigma(N_1 N_2 \rightarrow j_3 j_4 X_s) &= \frac{1}{2S^2} \prod_{X_3, X_4, X_s} (2\pi)^4 \delta^{(4)}(P_1^\mu + P_2^\mu - p_3^\mu - p_4^\mu - p_{X_s}^\mu) \\ &\times \sum_{IJ} C_I C_J^* \langle N_1 N_2 | O_J^\dagger | X_3, X_4, X_s \rangle \langle X_3, X_4, X_s | O_I | N_1 N_2 \rangle. \end{aligned} \quad (3)$$

Here \prod_{X_3, X_4, X_s} denotes the phase space for the final-state particles, and S is the hadronic center-of-mass energy squared. The set of operators O_I are the SCET operators for $2 \rightarrow 2$ processes and C_I are the Wilson coefficients obtained by matching SCET and full QCD [15, 16].

The operators can be categorized by the partons participating in the hard scattering processes. If the initial- and final-state particles consist of quarks or antiquarks, the set of the SCET collinear operators for $q\bar{q} \rightarrow q'\bar{q}'$ are given as

$$\mathcal{O}_1 = \bar{\chi}_2 T^a \gamma^\mu \chi_1 \cdot \bar{\chi}_4 T^a \gamma_\mu \chi_3, \quad \mathcal{O}_2 = \bar{\chi}_2 \gamma^\mu \chi_1 \cdot \bar{\chi}_4 \gamma_\mu \chi_3, \quad (4)$$

where the collinear fields $\chi = W^\dagger \xi$ are the collinear gauge-invariant combination with the collinear Wilson line W . The SU(3) generators T^a for the strong interaction are in the fundamental representation. These operators are responsible for the scattering of $q\bar{q} \rightarrow q\bar{q}$, $qq \rightarrow qq$, $\bar{q}\bar{q} \rightarrow \bar{q}\bar{q}$ including different types of quarks, which are related by the appropriate crossing symmetry.

For the processes $q\bar{q} \rightarrow gg$, $gg \rightarrow q\bar{q}$, $qq \rightarrow qq$ and $g\bar{q} \rightarrow g\bar{q}$, the relevant SCET collinear operators are given by¹

$$\mathcal{O}_1 = \bar{\chi}_2 T_a T_b \chi_1 B_{\perp 4}^{\mu a} B_{\perp \mu 3}^b, \quad \mathcal{O}_2 = \bar{\chi}_2 T_b T_a \chi_1 B_{\perp 4}^{\mu a} B_{\perp \mu 3}^b, \quad \mathcal{O}_3 = \bar{\chi}_2 \chi_1 B_{\perp 4}^{\mu a} B_{\perp \mu 3}^a, \quad (5)$$

where $B_{\perp i}^\mu = [W_i^\dagger i D_i^{\perp \mu} W_i]/g$ is the collinear gauge-invariant gluon field in the n_i direction in SCET. For the process $gg \rightarrow gg$, there are 9 independent collinear SCET operators, which are of the form $\mathcal{O}_i = T_i^{abcd} B_{\perp 2}^{\pm a} B_{\perp 1}^{\pm b} B_{\perp 4}^{\pm c} B_{\perp 3}^{\pm d}$ ($i = 1, \dots, 9$), where \pm indicates the helicity of the gluons. The explicit form can be found in Ref. [16].

The factorization procedure can be performed for any partonic processes, but it is illustrative to pick up one process and treat the factorization in detail. As a specific example, we consider the partonic process $q\bar{q} \rightarrow gg$. The relevant operators with the redefinition of the collinear fields to decouple the soft interaction $\chi \rightarrow Y\chi$, $B_{\perp \mu}^a \rightarrow \mathcal{Y}^{ab} B_{\perp \mu}^b$ are given by

$$O_I = \left(\bar{\chi}_2^\alpha \chi_1^\beta B_{\perp 4 \perp \mu}^a B_{\perp 3 \perp}^{b\mu} \right) \left(Y_2^\dagger \mathcal{Y}_4^{\dagger aa'} T_I^{a'b'} \mathcal{Y}_3^{b'b} Y_1 \right)_{\alpha\beta}, \quad (6)$$

¹ In Ref. [17], another independent set of operators are introduced: $\tilde{\mathcal{O}}_1 = \bar{\chi}_2 \chi_1 B_{\perp 4}^{\mu a} B_{\perp \mu 3}^a$, $\tilde{\mathcal{O}}_2 = d_{abc} \bar{\chi}_2 T_c \chi_1 B_{\perp 4}^{\mu a} B_{\perp \mu 3}^b$, and $\tilde{\mathcal{O}}_3 = i f_{abc} \bar{\chi}_2 T_c \chi_1 B_{\perp 4}^{\mu a} B_{\perp \mu 3}^b$. They are related by $\tilde{\mathcal{O}}_1 = \mathcal{O}_3$, $\tilde{\mathcal{O}}_2 = \mathcal{O}_1 + \mathcal{O}_2 - \mathcal{O}_3/N$, and $\mathcal{O}_3 = \mathcal{O}_1 - \mathcal{O}_2$.

where $T_1^{ab} = T^a T^b$, $T_2^{ab} = T^b T^a$ and $T_3^{ab} = \delta^{ab}$. The indices a, b (α, β) refer to the adjoint (fundamental) representation. The soft Wilson line Y_i associated with the n_i -collinear fermion is given in the fundamental representation, while the soft Wilson line \mathcal{Y}_i from the n_i -collinear gluon is given in the adjoint representation.

The collinear matrix element for the operators in Eq. (6) is given by

$$\sum_{X_3, X_4} \langle N_1 N_2 | \bar{\chi}_1^\rho \chi_2^\sigma B_{\perp 3}^{c\nu} B_{\perp 4\nu}^d | X_3 X_4 \rangle \langle X_3 X_4 | \bar{\chi}_2^\alpha \chi_1^\beta B_{\perp 4\mu}^a B_{\perp 3}^{b\mu} | N_1 N_2 \rangle, \quad (7)$$

and it can be expressed in terms of the gluon jet functions and the collinear distribution functions. The gluon jet functions in the n_3 and n_4 directions are defined as

$$\begin{aligned} \sum_{X_3} \langle 0 | B_{\perp 3}^{c\nu} | X_3 \rangle \Theta_J \langle X_3 | B_{\perp 3}^{b\mu} | 0 \rangle &= -g_\perp^{\mu\nu} \delta^{bc} \int \frac{d^4 p_3}{(2\pi)^3} J_g(p_3^2), \\ \sum_{X_4} \langle 0 | B_{\perp 4}^{d\nu} | X_4 \rangle \Theta_J \langle X_4 | B_{\perp 4}^{a\mu} | 0 \rangle &= -g_\perp^{\mu\nu} \delta^{ad} \int \frac{d^4 p_4}{(2\pi)^3} J_g(p_4^2), \end{aligned} \quad (8)$$

where Θ_J denotes the jet algorithm to be employed. The jet functions are normalized to $\delta(p_i^2)$ at tree level.

Near the threshold, the collinear distribution functions are defined as

$$\begin{aligned} \langle N_1 | \bar{\chi}_{1k}^\rho \delta\left(\xi_1 - \frac{\bar{n}_1 \cdot \mathcal{P}}{\bar{n}_1 \cdot P_1}\right) \chi_{1j}^\beta | N_1 \rangle &= \frac{\bar{n}_1 \cdot P_1}{2N} \left(\frac{\eta_1}{2}\right)_{jk} \delta^{\rho\beta} f_{q/N_1}(\xi_1), \\ \langle N_2 | \chi_{2l}^\sigma \delta\left(\xi_2 - \frac{\bar{n}_2 \cdot \mathcal{P}}{\bar{n}_2 \cdot P_2}\right) \bar{\chi}_{2i}^\alpha | N_2 \rangle &= \frac{\bar{n}_2 \cdot P_2}{2N} \left(\frac{\eta_2}{2}\right)_{li} \delta^{\sigma\alpha} f_{\bar{q}/N_2}(\xi_2), \end{aligned} \quad (9)$$

where the subscripts are the Dirac indices, and N is the number of colors. And \mathcal{P}^μ is the operator extracting the label momentum. The collinear distribution function is normalized as $\delta(1 - \xi)$ at tree level.

Then the dijet cross section near threshold is factorized as²

$$\sigma = \frac{1}{16\pi N^2 S} \sum_{IJ} H_{IJ}(\mu) S_{JI}(\mu) \int d\xi_1 f_{q/N_1}(\xi_1, \mu) \int d\xi_2 f_{\bar{q}/N_2}(\xi_2, \mu) \mathcal{J}_{g3} \mathcal{J}_{g4} + (q \leftrightarrow \bar{q}), \quad (10)$$

where the soft function S_{JI} is defined as

$$S_{JI} = \sum_{X_s} \text{tr} \langle 0 | Y_1^\dagger (\mathcal{Y}_3^\dagger T_J^\dagger \mathcal{Y}_4)^{ba} Y_2 | X_s \rangle \Theta_J \langle X_s | Y_2^\dagger (\mathcal{Y}_4^\dagger T_I \mathcal{Y}_3)^{ab} Y_1 | 0 \rangle, \quad (11)$$

with the appropriate jet algorithm denoted by Θ_J . The integrated jet function \mathcal{J}_{gi} is defined as

$$\mathcal{J}_{gi} = \int dp_i^2 J_g(p_i^2), \quad (i = 3, 4). \quad (12)$$

² To be rigorous, the effect of the Glauber gluons should be implemented to prove factorization.

If we are interested in the dijet invariant mass distribution $m_{j_3}^2 = (p_3 + l)^2$, $m_{j_4}^2 = (p_4 + l)^2$, the differential cross section with respect to the invariant jet masses is given by

$$\begin{aligned} \frac{d\sigma}{dm_{j_3}^2 dm_{j_4}^2} &= \frac{1}{16\pi N^2 S} \int d\xi_1 f_{q/N_1}(\xi_1, \mu) \int d\xi_2 f_{\bar{q}/N_2}(\xi_2, \mu) \\ &\times \int dl_+ dl_- J_g(m_{j_3}^2 - \bar{n} \cdot p_3 l_-) J_g(m_{j_4}^2 - \bar{n}_4 \cdot p_4 l_+) \sum_{IJ} H_{IJ} \tilde{S}_{JI}(l_+, l_-), \end{aligned} \quad (13)$$

with $l_+ = n_3 \cdot l$ and $l_- = n_4 \cdot l$. The differential soft function $\tilde{S}_{JI}(l_+, l_-)$ is defined as

$$\tilde{S}_{JI}(l_+, l_-) = \text{tr} \langle 0 | Y_1^\dagger (\mathcal{Y}_3^\dagger T_J^\dagger \mathcal{Y}_4)^{ba} Y_2 \delta(l_+ + n_3 \cdot \mathcal{P}_s) \Theta_J \delta(l_- + n_4 \cdot \mathcal{P}_s) Y_2^\dagger (\mathcal{Y}_4^\dagger T_I \mathcal{Y}_3)^{ab} Y_1 | 0 \rangle. \quad (14)$$

From now on, we concentrate on the integrated jet and soft functions at next-to-leading order. In probing the structure of divergence, it is necessary to analyze the phase space for the soft function in detail, and to discuss the calculational scheme in using the dimensional regularization.

III. PHASE SPACE AND DIVERGENCE OF THE SOFT FUNCTIONS

In disentangling the divergence structure, the soft function is the most sophisticated part to be treated with care. The phase space, in which the UV or IR divergence arises, depends on which Wilson lines are involved in the soft part. And there is some phase space missing due to the existence of the beam particles. On the technical side, we employ the dimensional regularization both for the UV and IR divergences, and we explain how we proceed especially when there are double poles. This section constitutes the main idea and technique in this paper.

A. Phase space for the soft function

At the parton level, the dijet production from hadron-hadron scattering and the process $e^+e^- \rightarrow 4$ jets are similar since they are related by the crossing symmetry. But in hadron-hadron scattering, only the final-state partons are organized by the jet algorithm, while all the final-state partons in $e^+e^- \rightarrow 4$ jets are scrutinized by the jet algorithm. This affects the soft function and its anomalous dimension, which depend on the jet cone size. However, it turns out that the anomalous dimension of the soft function depending on the jet cone size is diagonal in color basis, which cancels the cone size dependence of the anomalous dimension in the jet function.

We consider the cone-type jet algorithm at next-to-leading order, in which there are at most two particles inside a jet. At this order, we choose the jet axis in the n direction. The jet axis may be chosen as the thrust axis, or the weighted average of the rapidity and the azimuthal angle over the transverse energy. Then the particles inside a jet should satisfy the condition $\theta_i < R$. Here θ_i is the angle of the i -th particle with respect to the jet axis, and R is the jet cone size.

In the threshold region the jet algorithm can be expressed in terms of the lightcone momenta as follows [8, 14, 18]:

$$\begin{aligned}
\frac{n_3 \cdot l}{n_3 \cdot l + \bar{n}_3 \cdot l} &< \delta^2, \quad n_3 \text{ jet}, \\
\frac{n_4 \cdot l}{n_4 \cdot l + \bar{n}_4 \cdot l} &< \delta^2, \quad n_4 \text{ jet}, \\
n_3 \cdot l + n_4 \cdot l &< 2\beta Q, \quad \text{jet veto},
\end{aligned} \tag{15}$$

where $\delta = \tan(R/2)$. We retain this form with the understanding that R is actually replaced by $\mathcal{R}/\cosh y_J$, where \mathcal{R} is the cone size in the pseudorapidity-azimuthal angle space, and y_J is the pseudorapidity of the jet in hadron-hadron scattering [11]. And β is the fraction of the energy outside the jets acting as a jet veto, and $Q \approx \sqrt{S}$. The jet veto is needed to guarantee that the final states form a dijet event. The constraint due to this jet algorithm for the final-state particles is shown in Fig. 2 (a). Eq. (15) as a whole incorporates the jet algorithm. But when there is no confusion, we sometimes refer to the first two equations of Eq. (15) as the jet algorithm since they are the conditions for the particles to be inside the jet, and refer to the third equation as the jet veto.

For power counting in SCET, the n -collinear momentum scales as $p_n^\mu = (\bar{n} \cdot p, p_\perp, n \cdot p) \sim Q(1, \lambda, \lambda^2)$, where λ is the small parameter. Then the soft momentum scales as $p_s^\mu \sim Q(\lambda^2, \lambda^2, \lambda^2)$. And we also take $\delta \sim \mathcal{O}(\lambda)$ and $\beta \sim \mathcal{O}(\lambda^2)$ for definiteness. We may need other degrees of freedom if we are interested in the small R resummation [19]. But this topic will be deferred.

Though the phase space is constrained by the jet algorithm as shown in Fig. 2, the structure of the divergence depends on which soft Wilson lines participate in the soft function. The integrand in computing the real gluon emission can be obtained by expanding the

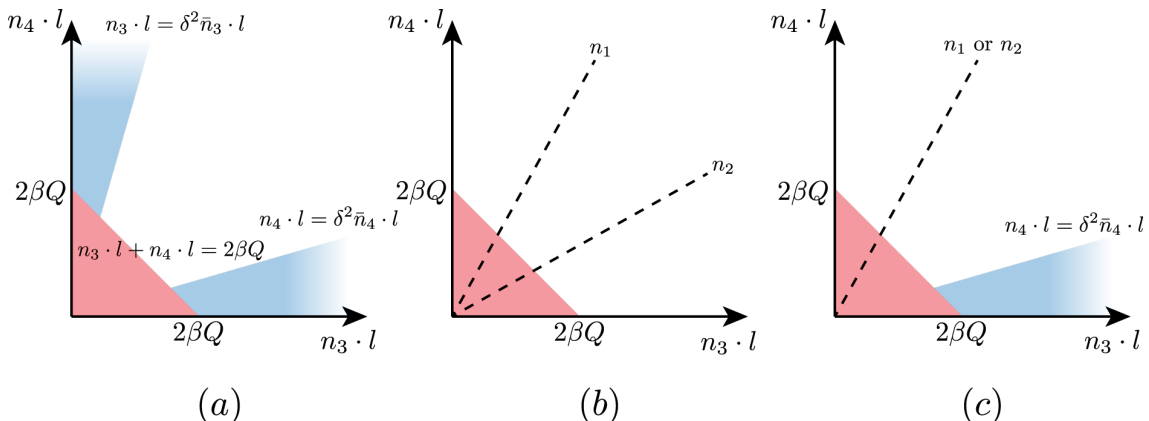


FIG. 2. The phase space for the soft function prescribed by the jet algorithm. The red region arises from the jet veto. (a) Jet-jet contribution: The blue region arises from the jet algorithm. The region close to the horizontal (vertical) axis corresponds to the jet in the n_4 (n_3) direction. (b) Beam-beam contribution: The dotted lines indicate the beam directions. (c) Beam-jet contributions: The phase space corresponds to the case $(i, j) = (1, 4)$ or $(2, 4)$. For $(i, j) = (1, 3)$ or $(2, 3)$, the blue region appears near the $n_4 \cdot l$ axis instead.

corresponding soft Wilson lines, and is of the form

$$I_{ij} = \frac{n_i \cdot n_j}{n_i \cdot l n_j \cdot l} \delta(l^2), \quad i, j = 1, \dots, 4. \quad (16)$$

The characteristics of I_{ij} are categorized into three classes: the jet-jet contribution $(i, j) = (3, 4)$, the beam-beam contribution $(i, j) = (1, 2)$, and the beam-jet contributions for the remaining combinations of (i, j) . The three classes have different structure of divergence.

For the jet-jet contribution $(i, j) = (3, 4)$, the denominator of I_{ij} becomes singular when the momentum l approaches zero or collinear to n_3 or n_4 . Therefore the UV or IR divergences arise in each of the phase space specified in Fig. 2 (a). However, when the virtual corrections are added, the soft part in the jet-jet contribution becomes IR finite [8].

For the beam-beam contribution $(i, j) = (1, 2)$, the denominator never becomes singular unless l approaches zero since the gluon momentum should be close to the jet directions n_3, n_4 , and away from the beam directions n_1, n_2 . Due to this fact, the contributions from the first two conditions of the jet algorithm in Eq. (15) (blue region) do not induce any (collinear) IR divergence and the contribution from that phase space is suppressed by $\delta^2 \sim \mathcal{O}(\lambda^2)$. The detailed calculation of the explicit contribution to order δ^2 is presented in Appendix A. Therefore the only divergence comes from the region specified by the jet veto, as illustrated in Fig. 2 (b), in which we show only the region of the phase space which yields the IR divergence. Here it is hard to visualize the $n_1 \cdot l$ and $n_2 \cdot l$ lines in Fig. 2 (b) and (c), so they are expressed as dashed lines for convenience. The contribution from the gluons in the n_1 and n_2 directions is critical in treating the IR divergence. This point will be discussed in detail.

For the beam-jet contributions, for example, $(i, j) = (1, 4)$ or $(2, 4)$, as shown in Fig. 2 (c), the denominator becomes singular when the momentum approaches zero or is collinear to n_4 . When the momentum is collinear to n_3 , the contribution is finite and suppressed by $\delta^2 \sim \mathcal{O}(\lambda^2)$ for the same reason as in the beam-beam contribution. Therefore the divergence occurs in the phase space, as illustrated in Fig. 2 (c). We can also consider the cases with $(i, j) = (1, 3)$ or $(2, 3)$, and the phase space which results in the IR divergence is given by the blue region near the $n_4 \cdot l$ axis instead along with the jet veto.

Considering the fact that the soft function from the jet-jet contributions with the virtual corrections is IR finite, we can see that the soft functions from the beam-jet and the beam-beam contributions should contain IR divergence because the IR divergence from the jet algorithms for the n_3 or n_4 jets or both is missing. This presents a predicament since the IR-divergent soft function loses its physical meaning. There must be another source for the IR divergence which cancels the existing divergence as mentioned above. That contribution is related to the emission of gluons exactly in the beam directions.

When a soft gluon is emitted outside the jet, its energy should be less than βQ according to the jet veto. The beam directions also belong to the region outside the jet. However, when a soft gluon is emitted exactly in the beam directions, that is, in the n_1 or n_2 directions, the jet topology also corresponds to a dijet event. In this case, the energy of the soft gluon can be larger than the jet veto, and this contribution should be added in calculating the soft function. In contrast, in e^+e^- annihilation, there is no such contribution since there

are no incoming hadrons in the beam direction. One of the main themes in this paper is to extract these contributions in order to show that the soft function becomes IR finite with this additional contribution.

We can consider a more general case away from the threshold, in which there are two central jets and two beam jets. Then the emission of soft gluons in the beam direction does not have to be exactly collinear to the incoming particles, and can be smeared to be inside the beam jets. Then it requires a beam algorithm analogous to the jet algorithm to treat the soft gluon in the beam directions. In this case, the anomalous dimensions may depend also on the size of the beam jets, and there may be nonglobal logarithms [20] related to the different sizes of the central jets and the beam jets. This may be interesting, but we will not consider this case here, and it is the topic to be pursued later. In a sense, the collinear distribution function in the dijet event near threshold corresponds to the beam function with the zero beam size.

B. Divergence structure and the dimensional regularization

Before we compute the soft functions, there are two important points which should be handled with care in using the dimensional regularization to separate the UV and the IR divergences. First, the ingredient to separate the UV and IR divergences is based on the fact that

$$\mu^\epsilon \int_0^\infty duu^{-1-\epsilon} = \frac{1}{\epsilon_{\text{UV}}} - \frac{1}{\epsilon_{\text{IR}}}, \quad (17)$$

where u has the dimension of a momentum. In the naive dimensional regularization in which the UV and IR divergences are not distinguished, the integral vanishes since it is a scaleless integral. The UV divergence is extracted as a pole in ϵ_{UV} by inserting an arbitrary IR regulator. Using the fact that the overall integral is zero, the IR divergence as a pole in ϵ_{IR} is obtained as in Eq. (17).

Secondly, in the virtual corrections of the soft functions, there appears an integral of the form

$$\begin{aligned} V_{ij} &= \left(\frac{\mu^2 e^\gamma}{4\pi}\right)^\epsilon \int \frac{d^D l}{(2\pi)^D} \frac{n_i \cdot n_j}{l^2 n_i \cdot l n_j \cdot l} \\ &= -\frac{i}{8\pi^2} \Gamma(1+\epsilon) \left(\frac{n_i \cdot n_j}{2}\right)^{-\epsilon} (\mu^2 e^\gamma)^\epsilon \int_0^\infty duu^{-1-\epsilon} \int_0^\infty dvv^{-1-\epsilon}. \end{aligned} \quad (18)$$

The only point we can claim about the integral is that it vanishes in the naive dimensional regularization, hence the integral is proportional to $1/\epsilon_{\text{UV}} - 1/\epsilon_{\text{IR}}$. Other than this observation, the result of the integration is ambiguous. To see why, let us consider two possible ways to compute this integral.

The first method is to treat the variables separately and it can be written as

$$\mu^{2\epsilon} \int_0^\infty duu^{-1-\epsilon} \int_0^\infty dvv^{-1-\epsilon} = \left(\mu^\epsilon \int_0^\infty duu^{-1-\epsilon}\right)^2 = \left(\frac{1}{\epsilon_{\text{UV}}} - \frac{1}{\epsilon_{\text{IR}}}\right)^2. \quad (19)$$

Then V_{ij} is given by

$$V_{ij} = -\frac{i}{8\pi^2} \left(\frac{1}{\epsilon_{\text{UV}}} - \frac{1}{\epsilon_{\text{IR}}} \right)^2. \quad (20)$$

On the other hand, the integral can also be performed by introducing the polar coordinates $u = r \cos \theta$, $v = r \sin \theta$, as

$$\begin{aligned} \mu^{2\epsilon} \int_0^\infty du u^{-1-\epsilon} \int_0^\infty dv v^{-1-\epsilon} &= \mu^{2\epsilon} \int_0^\infty dr r^{-1-2\epsilon} \int_0^{\pi/2} d\theta (\sin \theta \cos \theta)^{-1-\epsilon} \\ &= -\frac{1}{\epsilon_{\text{IR}}} \left(\frac{1}{\epsilon_{\text{UV}}} - \frac{1}{\epsilon_{\text{IR}}} \right). \end{aligned} \quad (21)$$

The integral on r yields both the UV and IR divergences, while the angular integral produces only the IR divergence. Therefore V_{ij} is given by

$$V_{ij} = \frac{i}{8\pi^2} \left(\frac{1}{\epsilon_{\text{UV}}} - \frac{1}{\epsilon_{\text{IR}}} \right) \left(\frac{1}{\epsilon_{\text{IR}}} - \ln \frac{n_i \cdot n_j}{2} \right). \quad (22)$$

Comparing Eqs. (19) and (21), the integrals are indeed proportional to $1/\epsilon_{\text{UV}} - 1/\epsilon_{\text{IR}}$, but they are different.

Now the question is which one should be employed in actual computations. We emphasize that the treatment of the virtual correction is not determined by the virtual correction alone, but is determined by how the real gluon emission is computed. The ambiguity of the divergences in the soft function was also pointed out in Refs. [21, 22]. The point is that the method in computing the virtual and the real contributions should be performed in the same way. Usually the real gluon emission is complicated when the jet algorithm is implemented. The phase space for the virtual correction is simpler than that of the real contribution, hence the computation is more versatile in the virtual correction. Thus we calculate the virtual correction in the same way as we compute the real gluon emission.

The argument can be justified as follows: If there is no constraint for the soft gluon emission, the whole phase space is covered, and the contribution is proportional to V_{ij} . The virtual correction has the same form as the real gluon emission except the sign. The whole soft contribution at one loop, as well as all the divergences, vanishes as long as we maintain the same method of calculation either Eq. (19) or Eq. (21). Actually the inclusive soft function for the real gluon emission receives no radiative corrections to all orders. If we employ different methods for the virtual and real corrections, the result cannot be zero. This argument also holds for the computation of the soft function with the jet algorithm. The correct divergence structure is obtained only when the same method is applied consistently to the virtual and the real contributions.

The question remains whether the final finite answer could be the same irrespective of the different treatment for V_{ij} . The jet-jet contribution has been computed using Eq. (19) in Ref. [8], and we will show here that the same answer is obtained using Eq. (21) with the angular integral in the real gluon emission. Note also that the different divergence structure in Eqs. (19) and (21) arises only when the whole phase space is covered. In other cases in which the whole phase space is not involved, for example, in the contribution from the jet veto as shown in Fig. 2 (b), the integration of Eq. (18) is the same in both approaches producing only the IR divergence.

IV. SOFT FUNCTION

The soft function, defined in Eq. (11), is given again by

$$S_{JI} = \sum_{X_s} \text{tr} \langle 0 | Y_1^\dagger (\mathcal{Y}_3^\dagger T_J^\dagger \mathcal{Y}_4)^{ba} Y_2 | X_s \rangle \Theta_J \langle X_s | Y_2^\dagger (\mathcal{Y}_4^\dagger T_I \mathcal{Y}_3)^{ab} Y_1 | 0 \rangle. \quad (23)$$

The Wilson lines Y_2^\dagger and Y_1 correctly describe the soft gluon emission from the antiquark and the quark in the initial state. But, to be exact, the Wilson lines \mathcal{Y}_4^\dagger and \mathcal{Y}_3 should be $\tilde{\mathcal{Y}}_4^\dagger$ and $\tilde{\mathcal{Y}}_3$, describing the soft gluon emission from the outgoing particles [23]. However, we keep the forms as they are for notational simplicity. The soft Wilson lines are given as

$$Y_1 = \sum_{\text{perm.}} \exp \left[\frac{1}{n_1 \cdot \mathcal{R} + i0} (-gn_1 \cdot A_s) \right], \quad Y_2^\dagger = \sum_{\text{perm.}} \exp \left[-gn_2 \cdot A_s \frac{1}{n_2 \cdot \mathcal{R}^\dagger - i0} \right],$$

$$\mathcal{Y}_3 = \sum_{\text{perm.}} \exp \left[\frac{1}{n_3 \cdot \mathcal{R} - i0} (-gn_3 \cdot A_s) \right], \quad \mathcal{Y}_4^\dagger = \sum_{\text{perm.}} \exp \left[-gn_4 \cdot A_s \frac{1}{n_4 \cdot \mathcal{R}^\dagger + i0} \right], \quad (24)$$

where \mathcal{R} is the operator extracting the soft momentum.

The Feynman diagrams for the soft function at one loop is shown in Fig. 3. Figs. 3 (a) and (b) represent the virtual and the real corrections respectively. The vertical dashed lines are the unitarity cuts, and the hermitian conjugates are not shown. The contributions for the soft function can be expressed as the sum of the two parts, one from the jet veto and the other from the jet algorithm. These are given as

$$M_{ij}^{\text{veto}} = 2\pi g^2 \left(\frac{\mu^2 e^\gamma}{4\pi} \right)^\epsilon \int \frac{d^D l}{(2\pi)^D} \frac{n_i \cdot n_j}{n_i \cdot l n_j \cdot l} \delta(l^2) \Theta(0 < l_0 < \beta Q),$$

$$M_{ij}^{\text{jet}} = 2\pi g^2 \left(\frac{\mu^2 e^\gamma}{4\pi} \right)^\epsilon \int \frac{d^D l}{(2\pi)^D} \frac{n_i \cdot n_j}{n_i \cdot l n_j \cdot l} \delta(l^2) \Theta(l_0 > \beta Q) \Theta_J, \quad (25)$$

apart from the group theory factors $-\mathbf{T}_i \cdot \mathbf{T}_j$ [17, 24, 25]. The jet algorithm Θ_J represents either of the first two equations in Eq. (15) depending on whether the jet in the n_3 or n_4 direction is considered. M_{ij}^{veto} (M_{ij}^{jet}) is the contribution from the phase space colored as red (blue) in Fig. 2.

Since M_{ij}^{jet} will be computed using the angular integral, the virtual correction with Eq. (21) is given by

$$M_{ij}^V = -ig^2 V_{ij} = \frac{\alpha_s}{2\pi} \left[-\frac{1}{\epsilon_{\text{IR}}^2} + \frac{1}{\epsilon_{\text{UV}} \epsilon_{\text{IR}}} - \left(\frac{1}{\epsilon_{\text{UV}}} - \frac{1}{\epsilon_{\text{IR}}} \right) \ln \frac{n_{ij}}{2} \right], \quad (26)$$



FIG. 3. Feynman diagrams for the soft function at one loop. (a) Virtual correction (b) Real gluon emission. The hermitian conjugates are omitted. The dashed lines are the unitarity cuts.

where $n_{ij} = n_i \cdot n_j$.

A. Jet-jet contribution

This is the contribution from the case $(i, j) = (3, 4)$, where the soft gluons are emitted from the soft Wilson lines associated with the final-state partons. The results are given by

$$\begin{aligned}
M_{34}^{\text{veto}} &= \frac{\alpha_s}{2\pi} \left[\frac{1}{\epsilon_{\text{IR}}^2} + \frac{1}{\epsilon_{\text{IR}}} \left(2 \ln \frac{\mu}{2\beta Q} - \ln \frac{n_{34}}{2} \right) + 2 \ln^2 \frac{\mu}{2\beta Q} \right. \\
&\quad \left. - 2 \ln \frac{\mu}{2\beta Q} \ln \frac{n_{34}}{2} - \text{Li}_2 \left(1 - \frac{2}{n_{34}} \right) - \frac{\pi^2}{4} \right], \\
M_{34}^{\text{jet}} &= \frac{\alpha_s}{2\pi} \left(-\frac{1}{2\epsilon_{\text{UV}}\epsilon_{\text{IR}}} - \frac{1}{\epsilon_{\text{IR}}} \ln \frac{\mu}{2\beta Q} + \frac{1}{\epsilon_{\text{UV}}} \ln \delta - \ln^2 \frac{\mu}{2\beta Q \delta} + \frac{\pi^2}{24} \right), \tag{27}
\end{aligned}$$

where n_{34} is kept explicitly for comparison with other cases. Note that the computation of each term in Eq. (27) is performed using the angular integral in the phase space based on Eq. (21). The detailed calculation is presented in Appendix A. Since the phase space for the jet veto depends on the directions of n_i and n_j (n_3 and n_4 in this case) in general, M_{ij}^{veto} depends on n_{ij} . However, the jet contribution M_{ij}^{jet} collects the contribution in a single jet direction, hence it depends not on n_{ij} but only on δ , and the jet veto parameter β .

The soft contribution in the jet-jet contribution is given by

$$\begin{aligned}
M_{34} &= M_{34}^{\text{veto}} + 2M_{34}^{\text{jet}} + M_{34}^V \\
&= \frac{\alpha_s}{2\pi} \left[\left(\frac{1}{\epsilon_{\text{UV}}} + 2 \ln \frac{\mu}{2\beta Q} \right) \ln \frac{2\delta^2}{n_{34}} - 2 \ln^2 \delta - \text{Li}_2 \left(1 - \frac{2}{n_{34}} \right) - \frac{\pi^2}{6} \right] \\
&= \frac{\alpha_s}{2\pi} \left[2 \left(\frac{1}{\epsilon_{\text{UV}}} + 2 \ln \frac{\mu}{2\beta Q} \right) \ln \delta - 2 \ln^2 \delta - \frac{\pi^2}{6} \right], \tag{28}
\end{aligned}$$

where the last line is obtained by putting $n_{34} = 2$. The soft contributions to order δ^2 at order α_s are computed in detail in Appendix A. For the jet-jet contribution, it is given by

$$M_{34}(\delta^2) = \frac{\alpha_s}{\pi} \delta^2. \tag{29}$$

The same result is obtained by computing each term based on Eq. (19) [8]. This verifies the point that the divergences as well as the finite terms are the same in the two approaches as long as a consistent method is employed in the virtual and real contributions. The finite soft contribution at order α_s is given as

$$\mathcal{M}_{34}^{(1)} = \frac{\alpha_s}{2\pi} \left(4 \ln \frac{\mu}{2\beta Q} \ln \delta - 2 \ln^2 \delta - \frac{\pi^2}{6} \right). \tag{30}$$

B. Beam-beam contribution

The beam-beam contribution corresponds to the case $(i, j) = (1, 2)$. The jet contribution M_{12}^{jet} is finite and suppressed by δ^2 , hence neglected. However, it is explicitly computed in

Appendix A . The contribution M_{12}^{veto} is given by

$$M_{12}^{\text{veto}} = \frac{\alpha_s}{2\pi} \left[\frac{1}{\epsilon_{\text{IR}}^2} + \frac{1}{\epsilon_{\text{IR}}} \left(2 \ln \frac{\mu}{2\beta Q} - \ln \frac{n_{12}}{2} \right) + 2 \ln^2 \frac{\mu}{2\beta Q} - 2 \ln \frac{\mu}{2\beta Q} \ln \frac{n_{12}}{2} - \text{Li}_2 \left(1 - \frac{2}{n_{12}} \right) - \frac{\pi^2}{4} \right]. \quad (31)$$

Here the dependence of n_{12} is retained but the final result is obtained by putting $n_{12} = 2$. Obviously, this is the same as M_{34}^{veto} .

Note that the sum of M_{12}^{veto} and the virtual correction M_{12}^V is still IR divergent, which is given by

$$M_{12}^{\text{veto}} + M_V = \frac{\alpha_s}{2\pi} \left(\frac{1}{\epsilon_{\text{UV}}\epsilon_{\text{IR}}} + \frac{2}{\epsilon_{\text{IR}}} \ln \frac{\mu}{2\beta Q} + 2 \ln^2 \frac{\mu}{2\beta Q} - \frac{\pi^2}{4} \right). \quad (32)$$

As explained in Sec. III A, we should add the contribution M^{beam} from the real gluon emission in the beam direction with $l_0 > \beta Q$. It is given by

$$M^{\text{beam}} = \frac{\alpha_s}{2\pi} \left(-\frac{1}{2\epsilon_{\text{UV}}\epsilon_{\text{IR}}} - \frac{1}{\epsilon_{\text{IR}}} \ln \frac{\mu}{2\beta Q} - \ln^2 \frac{\mu}{2\beta Q} + \frac{\pi^2}{24} \right). \quad (33)$$

The detailed derivation of M_{beam} is presented in Appendix B 1.

The beam-beam contribution for the soft part at one loop can be obtained by setting $n_{12} = 2$, and it is given by

$$M_{12} = M_{12}^{\text{veto}} + M_{12}^V + 2M^{\text{beam}} = \frac{\alpha_s}{2\pi} \left[-\left(\frac{1}{\epsilon_{\text{UV}}} + 2 \ln \frac{\mu}{2\beta Q} \right) \ln \frac{n_{12}}{2} - \text{Li}_2 \left(1 - \frac{2}{n_{12}} \right) - \frac{\pi^2}{6} \right] = \frac{\alpha_s}{2\pi} \left(-\frac{\pi^2}{6} \right). \quad (34)$$

Since it is IR finite, M_{12} gives the finite soft contribution at one loop as

$$\mathcal{M}_{12}^{(1)} = \frac{\alpha_s}{2\pi} \left(-\frac{\pi^2}{6} \right). \quad (35)$$

In addition, the contribution at order δ^2 and α_s is given by

$$M_{12}(\delta^2) = \frac{\alpha_s}{\pi} \frac{2\delta^2}{n_{13}n_{23}} \left(1 + \frac{1}{\epsilon_{\text{UV}}} + 2 \ln \frac{\mu}{2\beta Q\delta} \right). \quad (36)$$

C. Beam-jet contribution

This corresponds to the cases (i, j) with $i = 1, 2$ and $j = 3, 4$. The results are given by

$$M_{ij}^{\text{veto}} = \frac{\alpha_s}{2\pi} \left[\frac{1}{\epsilon_{\text{IR}}^2} + \frac{1}{\epsilon_{\text{IR}}} \left(2 \ln \frac{\mu}{2\beta Q} - \ln \frac{n_{ij}}{2} \right) + 2 \ln^2 \frac{\mu}{2\beta Q} - 2 \ln \frac{\mu}{2\beta Q} \ln \frac{n_{ij}}{2} - \text{Li}_2 \left(1 - \frac{2}{n_{ij}} \right) - \frac{\pi^2}{4} \right],$$

$$M_{ij}^{\text{jet}} = \frac{\alpha_s}{2\pi} \left(-\frac{1}{2\epsilon_{\text{UV}}\epsilon_{\text{IR}}} - \frac{1}{\epsilon_{\text{IR}}} \ln \frac{\mu}{2\beta Q} + \frac{1}{\epsilon_{\text{UV}}} \ln \delta - \ln^2 \frac{\mu}{2\beta Q\delta} + \frac{\pi^2}{24} \right). \quad (37)$$

The contribution M_{ij}^{veto} can be computed exactly in the same way as S_{ij}^{incl} in Ref. [18] by replacing the pole ϵ by ϵ_{IR} . This is because M_{ij}^{veto} contains only the IR divergence due to the phase space constraint. In computing M_{ij}^{jet} , care must be taken to separate the IR and UV divergences, and the detailed computation is presented in Appendix A.

Without the soft contribution in the beam direction, the soft part still remains IR divergent. This intermediate soft contribution is given by

$$M_{ij}^{\text{veto}} + M_{ij}^{\text{jet}} + M_{ij}^V = \frac{\alpha_s}{2\pi} \left[\frac{1}{2\epsilon_{\text{UV}}\epsilon_{\text{IR}}} + \frac{1}{\epsilon_{\text{IR}}} \ln \frac{\mu}{2\beta Q} + \ln^2 \frac{\mu}{2\beta Q} + \frac{1}{\epsilon_{\text{UV}}} \ln \frac{2\delta}{n_{ij}} \right. \\ \left. + 2 \ln \frac{\mu}{2\beta Q} \ln \frac{2\delta}{n_{ij}} - \ln^2 \delta - \text{Li}_2\left(1 - \frac{2}{n_{ij}}\right) - \frac{5}{24}\pi^2 \right]. \quad (38)$$

It turns out that the beam contribution M^{beam} is the same both in the beam-beam and in the beam-jet contributions. This is explained in detail in Appendix B. Finally the soft part in the beam-jet contribution including the beam contribution is given by

$$M_{ij} = M_{ij}^{\text{veto}} + M_{ij}^{\text{jet}} + M_{ij}^V + M^{\text{beam}} \\ = \frac{\alpha_s}{2\pi} \left[\left(\frac{1}{\epsilon_{\text{UV}}} + 2 \ln \frac{\mu}{2\beta Q} \right) \ln \frac{2\delta}{n_{ij}} - \ln^2 \delta - \text{Li}_2\left(1 - \frac{2}{n_{ij}}\right) - \frac{\pi^2}{6} \right], \quad (39)$$

which is IR finite.

The soft contribution for the beam-jet case at one loop is given by

$$\mathcal{M}_{ij}^{(1)} = \frac{\alpha_s}{2\pi} \left[2 \ln \frac{2\delta}{n_{ij}} \ln \frac{\mu}{2\beta Q} - \ln^2 \delta - \text{Li}_2\left(1 - \frac{2}{n_{ij}}\right) - \frac{\pi^2}{6} \right]. \quad (40)$$

And the suppressed term proportional to δ^2 , using the jet algorithm for the n_k -jet at order α_s is given as

$$M_{ij}^k(\delta^2) = \begin{cases} \frac{\alpha_s}{2\pi} \delta^2 \left[1 + \frac{2 - n_{ij}}{n_{ij}} \left(\frac{3}{2} + \frac{1}{2\epsilon_{\text{UV}}} + \ln \frac{\mu}{2\beta Q \delta} \right) \right], & k = j, \\ \frac{\alpha_s}{2\pi} \delta^2 \frac{n_{ij}}{n_{ik}n_{jk}} \left(1 + \frac{1}{\epsilon_{\text{UV}}} + 2 \ln \frac{\mu}{2\delta\beta Q} \right), & k \neq j. \end{cases} \quad (41)$$

V. GLUON JET FUNCTION

The inclusive gluon jet function has been computed to one-loop order [26], and two-loop order [27]. Here we compute the gluon jet function with the cone jet algorithm at one loop. The cone jet algorithm at next-to-leading order involves at most two particles inside a jet. In computing the jet function, the matrix element squared is schematically shown in Fig. 4. The loop includes other particles. (See Fig. 6.) If we make a unitarity cut in any of the gluon lines, the cut gluon lines correspond to the final-state particles. For example, if a single leg is cut, it represents a single final-state particle with the virtual correction. If the loop is cut, it represents two final-state particles, to which the jet algorithm is applied.

The momentum of the jet is given by p , and the momenta of the two gluons are labeled as l and $p - l$ respectively. Suppose that the jet is collinear in the n lightcone direction.

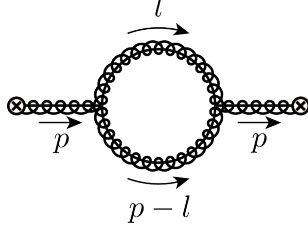


FIG. 4. Assignment of the momenta for the final-state gluons.

Then the momenta of the gluons can be written as

$$p_1 = (l_-, l_\perp, l_+), \quad p_2 = (Q - l_-, -l_\perp, p^2/Q - l_+), \quad (42)$$

where $Q = \bar{n} \cdot p = p_-$. The energies of the gluons and the invariant mass squared of the jet are given by

$$E_1 = \frac{1}{2}(l_- + l_+), \quad E_2 = \frac{1}{2}(Q - l_- + \frac{p^2}{Q} - l_+), \quad p^2 = \frac{Ql_+}{1 - l_-/Q}. \quad (43)$$

The cone jet algorithm for the n -collinear jet requires $\theta_1 < R$ and $\theta_2 < R$, where R is the jet cone size, and θ_i is the angle of the gluon i with respect to the jet axis, which is chosen to be in the n direction. This jet algorithm for the collinear part can be written as [8, 14, 18]

$$\Theta_J = \Theta\left(\delta^2 > \frac{l_+}{l_-}\right)\Theta\left(l_- < \frac{Q}{2}\right) + \Theta\left(\delta^2 > \frac{l_-l_+}{(Q-l_-)^2}\right)\Theta\left(l_- > \frac{Q}{2}\right) \quad (44)$$

where $\delta = \tan R/2$. The two final-state particles should satisfy both $\theta_1 < R$ and $\theta_2 < R$. However, if $E_1 < E_2$, that is, if $l_- < Q/2$, when the constraint $\theta_1 < R$ is satisfied, the condition $\theta_2 < R$ is automatically satisfied, and vice versa. This fact is implemented in the jet algorithm, Eq. (44).

The above jet algorithm includes the soft modes when $l_- \rightarrow 0$ for p_1 or $l_- \rightarrow Q$ for p_2 . The zero-bin subtraction should be employed to subtract the soft contribution from the jet function to avoid double counting [28]. If we switch p_1 and p_2 in Eq. (44), the two terms are switched to give the same result. And the calculation involved in the jet function is

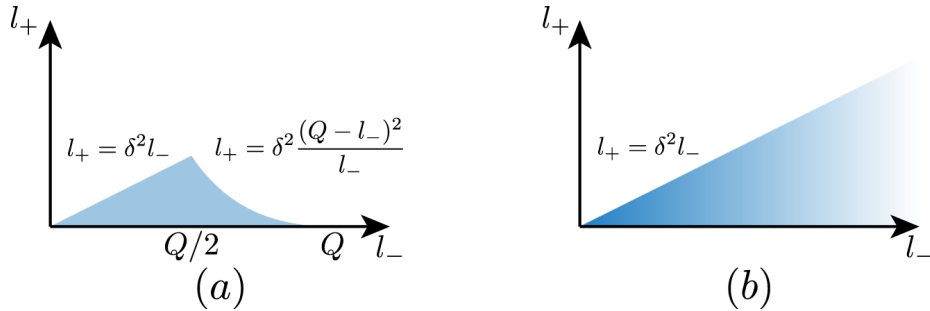


FIG. 5. Phase space for the n -collinear jet function. (a) Naive collinear contribution, (b) Zero-bin contribution in the limit $l_- \rightarrow 0$. Another limit $l_- \rightarrow Q$ gives the same result.

also invariant under this switch since the final-state particles are identical. Therefore the zero-bin contribution is obtained by choosing the jet algorithm for the zero-bin contribution from the first term in Eq. (44) with $l_- \rightarrow 0$, and we multiply it by two to get the final answer. With this in mind, the jet algorithm for the zero-bin contribution is given by

$$\Theta_J^0 = \Theta\left(\delta^2 > \frac{l_+}{l_-}\right). \quad (45)$$

The phase spaces for the naive collinear contribution and the zero-bin contribution are shown in Fig. 5 (a), (b) respectively. Here we consider the integrated gluon jet function \mathcal{J}_g .

We present the result with the prescription given by Eq. (19) in computing the zero-bin contributions. As we will see in Eq. (53), when the result is IR finite, we obtain the same result whichever prescriptions we employ as long as the same prescription is applied to the virtual and the real contributions.

The Feynman diagrams for the gluon jet function at one loop are shown in Fig. 6. Figs. 6 (a) and (b) are the virtual and real corrections from the Wilson lines. Figs. 6 (c)–(e) are the cut diagrams for a fermion, a gluon and a ghost loop respectively. The vertical dashed lines represent the unitarity cuts.

The naive collinear and zero-bin contributions from Fig. 6 (a) are given as

$$\begin{aligned} \tilde{M}_a &= \frac{ig^2 C_A}{2} \left(\frac{\mu^2 e^\gamma}{4\pi}\right)^\epsilon \int \frac{d^D l}{(2\pi)^D} \frac{1}{l^2(p-l)^2} \left(\frac{Q+l_-}{Q-l_-} + \frac{2Q-l_-}{l_-}\right) \\ &= \frac{\alpha_s C_A}{4\pi} \left(\frac{1}{\epsilon_{UV}} - \frac{1}{\epsilon_{IR}}\right) \left(\frac{2}{\epsilon_{IR}} + 1 + 2 \ln \frac{\mu}{Q}\right), \\ M_a^0 &= -2ig^2 C_A \left(\frac{\mu^2 e^\gamma}{4\pi}\right)^\epsilon \int \frac{d^D l}{(2\pi)^D} \frac{1}{l^2 l_- l_+} = -\frac{\alpha_s C_A}{2\pi} \left(\frac{1}{\epsilon_{UV}} - \frac{1}{\epsilon_{IR}}\right)^2, \end{aligned} \quad (46)$$

and the net contribution is given as

$$M_a = \tilde{M}_a - M_a^0 = \frac{\alpha_s C_A}{4\pi} \left(\frac{1}{\epsilon_{UV}} - \frac{1}{\epsilon_{IR}}\right) \left(\frac{2}{\epsilon_{UV}} + 1 + 2 \ln \frac{\mu}{Q}\right). \quad (47)$$

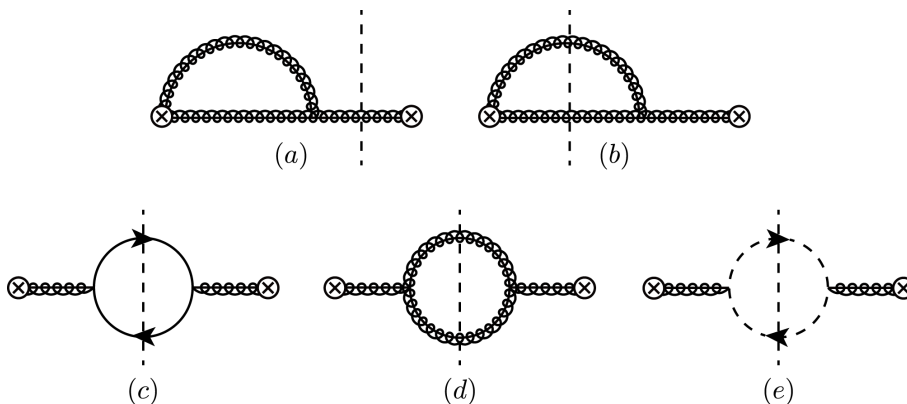


FIG. 6. Feynman diagrams for the gluon jet function. Curly lines are gluons, solid lines with arrows are fermions, dashed lines with arrows are ghost particles. The vertical dashed lines represent the unitarity cut. (a) Virtual correction (b) real gluon emission, and the mirror images are omitted. The remainder represents the contributions from the cuts of (c) a fermion loop (d) a gluon loop and (e) a ghost loop. The diagrams for the wave function renormalization are omitted.

The naive collinear contribution from Fig. 6 (b) is given by

$$\begin{aligned}\tilde{M}_b &= \frac{\alpha_s C_A}{8\pi Q} \frac{(\mu^2 e^\gamma)^\epsilon}{\Gamma(1-\epsilon)} \int dl_- dl_+ l_+^{-1-\epsilon} l_-^{-\epsilon} \left(\frac{Q+l_-}{Q-l_-} + \frac{2Q-l_-}{l_-} \right) \Theta_J \\ &= \frac{\alpha_s C_A}{4\pi} \left[\frac{1}{\epsilon_{\text{IR}}^2} + \frac{1}{\epsilon_{\text{IR}}} \left(1 + 2 \ln \frac{\mu}{Q\delta} \right) + 2 \ln \frac{\mu}{Q\delta} + 2 \ln^2 \frac{\mu}{Q\delta} + 2 + 2 \ln 2 - \frac{5}{12} \pi^2 \right].\end{aligned}\quad (48)$$

The zero-bin contribution, using Eq. (45), is given as

$$M_b^0 = \frac{\alpha_s C_A}{2\pi} \frac{(\mu^2 e^\gamma)^\epsilon}{\Gamma(1-\epsilon)} \int_0^\infty dl_- l_-^{-1-\epsilon} \int_0^{\delta^2 l_-} dl_+ l_+^{-1-\epsilon}.\quad (49)$$

In order to extract the UV and IR divergences correctly, we calculate the integral in the following way with $l_- = \mu x$, $l_+ = \mu y$ as

$$\begin{aligned}& \int_0^\infty dx x^{-1-\epsilon} \int_0^{x\delta^2} dy y^{-1-\epsilon} \\ &= \int_0^a dx x^{-1-\epsilon} \int_0^{x\delta^2} dy y^{-1-\epsilon} + \int_a^\infty dx x^{-1-\epsilon} \left(\int_0^\infty dy y^{-1-\epsilon} - \int_{x\delta^2}^\infty dy y^{-1-\epsilon} \right) \\ &= \frac{1}{2} \left(\frac{1}{\epsilon_{\text{UV}}} - \frac{1}{\epsilon_{\text{IR}}} \right) \left(\frac{1}{\epsilon_{\text{UV}}} - \frac{1}{\epsilon_{\text{IR}}} + \ln \delta^2 \right),\end{aligned}\quad (50)$$

where a is some positive number, which facilitates the separation of the UV and IR divergences. And the final result is independent of a .

The zero-bin contribution is given by

$$M_b^0 = \frac{\alpha_s C_A}{4\pi} \left[\left(\frac{1}{\epsilon_{\text{UV}}} - \frac{1}{\epsilon_{\text{IR}}} \right)^2 + \left(\frac{1}{\epsilon_{\text{UV}}} - \frac{1}{\epsilon_{\text{IR}}} \right) \ln \delta^2 \right],\quad (51)$$

and the net contribution is given as

$$\begin{aligned}M_b = \tilde{M}_b - M_b^0 &= \frac{\alpha_s C_A}{4\pi} \left[-\frac{1}{\epsilon_{\text{UV}}^2} + \frac{2}{\epsilon_{\text{UV}} \epsilon_{\text{IR}}} - \frac{1}{\epsilon_{\text{UV}}} \ln \delta^2 + \frac{1}{\epsilon_{\text{IR}}} \left(1 + 2 \ln \frac{\mu}{Q} \right) \right. \\ &\quad \left. + 2 \ln \frac{\mu}{Q\delta} + 2 \ln^2 \frac{\mu}{Q\delta} + 2 + 2 \ln 2 - \frac{5}{12} \pi^2 \right].\end{aligned}\quad (52)$$

If we add M_a and M_b , we obtain the IR finite result:

$$M_a + M_b = \frac{\alpha_s C_A}{4\pi} \left[\frac{1}{\epsilon_{\text{UV}}^2} + \frac{1}{\epsilon_{\text{UV}}} \left(1 + 2 \ln \frac{\mu}{Q\delta} \right) + 2 \ln \frac{\mu}{Q\delta} + 2 \ln^2 \frac{\mu}{Q\delta} + 2 + 2 \ln 2 - \frac{5}{12} \pi^2 \right].\quad (53)$$

The loops in Figs. 6 (c)-(e) consist of fermions, gluons and ghost particles respectively. The zero-bin contributions are power suppressed compared to the naive collinear contributions, thus neglected. The naive collinear contributions from the fermions, the gluons and

the ghost particles are given respectively by

$$\begin{aligned}
\tilde{M}_f &= \frac{\alpha_s T_F n_f}{2\pi Q} \frac{(\mu^2 e^\gamma)^\epsilon}{\Gamma(1-\epsilon)} \int dl_- dl_+ l_-^{2-\epsilon} \left(1 - \frac{l_-}{Q}\right)^2 l_+^{-1-\epsilon} \\
&\quad \times \left[\left(\frac{1}{l_-} + \frac{1}{Q-l_-} \right)^2 - \frac{2}{1-\epsilon} \frac{1}{l_-(Q-l_-)} \right] \Theta_J \\
&= \frac{\alpha_s T_F n_f}{4\pi} \left(-\frac{4}{3\epsilon_{\text{IR}}} - \frac{8}{3} \ln \frac{\mu}{Q\delta} - \frac{23}{9} - \frac{8}{3} \ln 2 \right), \\
\tilde{M}_g &= -\frac{\alpha_s C_A}{8\pi Q} \frac{(\mu^2 e^\gamma)^\epsilon}{\Gamma(1-\epsilon)} \int dl_- dl_+ \left[4l_-^\epsilon l_+^{1-\epsilon} - \frac{5-4\epsilon}{1-\epsilon} l_-^{1-\epsilon} \left(1 - \frac{l_-}{Q}\right) \frac{l_+^{-1-\epsilon}}{Q} \right] \Theta_J \\
&= \frac{\alpha_s C_A}{8\pi} \left(\frac{19}{6\epsilon_{\text{IR}}} + \frac{19}{3} \ln \frac{\mu}{Q\delta} + \frac{247}{36} + \frac{19}{3} \ln 2 \right), \\
\tilde{M}_{\text{ghost}} &= -\frac{\alpha_s C_A}{8\pi Q^2} \frac{(\mu^2 e^\gamma)^\epsilon}{\Gamma(2-\epsilon)} \int dl_- dl_+ l_-^{1-\epsilon} \left(1 - \frac{l_-}{Q}\right) l_+^{-1-\epsilon} \Theta_J \\
&= \frac{\alpha_s C_A}{8\pi} \left(\frac{1}{6\epsilon_{\text{IR}}} + \frac{1}{3} \ln \frac{\mu}{Q\delta} + \frac{13}{36} + \frac{1}{3} \ln 2 \right), \tag{54}
\end{aligned}$$

where n_f is the number of quark flavors. The total contribution is given by

$$\begin{aligned}
\tilde{M}_f + \tilde{M}_g + \tilde{M}_{\text{ghost}} &= \frac{\alpha_s}{4\pi} \left[\left(\frac{5}{3} C_A - \frac{4}{3} T_F n_f \right) \left(\frac{1}{\epsilon_{\text{IR}}} + 2 \ln \frac{\mu}{Q\delta} \right) \right. \\
&\quad \left. + \frac{65}{18} C_A - \frac{23}{9} T_F n_f + 2 \left(\frac{5}{3} C_A - \frac{4}{3} T_F n_f \right) \ln 2 \right]. \tag{55}
\end{aligned}$$

Finally, the gluon field-strength renormalization at one loop is given by

$$Z_g^{(1)} = \frac{\alpha_s}{4\pi} \left(\frac{1}{\epsilon_{\text{UV}}} - \frac{1}{\epsilon_{\text{IR}}} \right) \left(\frac{5}{3} C_A - \frac{4}{3} T_F n_f \right). \tag{56}$$

The overall contribution of the real and virtual corrections from the gluon self energy at order α_s is given by

$$\begin{aligned}
M_{\text{self}} &= \frac{\alpha_s}{4\pi} \left[\left(\frac{5}{3} C_A - \frac{4}{3} T_F n_f \right) \left(\frac{1}{\epsilon_{\text{UV}}} + 2 \ln \frac{\mu}{Q\delta} \right) \right. \\
&\quad \left. + \frac{65}{18} C_A - \frac{23}{9} T_F n_f + 2 \left(\frac{5}{3} C_A - \frac{4}{3} T_F n_f \right) \ln 2 \right]. \tag{57}
\end{aligned}$$

The total collinear contributions are given by

$$\begin{aligned}
M_{\text{coll}} &= 2(M_a + M_b) + M_{\text{self}} \\
&= \frac{\alpha_s}{2\pi} \left[\frac{C_A}{\epsilon_{\text{UV}}^2} + \frac{1}{\epsilon_{\text{UV}}} \left(\frac{\beta_0}{2} + 2C_A \ln \frac{\mu}{Q\delta} \right) + \beta_0 \ln \frac{\mu}{Q\delta} + 2C_A \ln^2 \frac{\mu}{Q\delta} \right. \\
&\quad \left. + \frac{137}{36} C_A - \frac{23}{18} T_F n_f + \beta_0 \ln 2 - \frac{5}{12} C_A \pi^2 \right], \tag{58}
\end{aligned}$$

where $\beta_0 = 11C_A/3 - 4T_F n_f/3$ is the leading term of the QCD beta function. The collinear contribution is clearly IR finite, and the gluon jet function at one loop is obtained by adding the counterterms as

$$\mathcal{J}_g^{(1)} = \frac{\alpha_s}{2\pi} \left(\beta_0 \ln \frac{\mu}{Q\delta} + 2C_A \ln^2 \frac{\mu}{Q\delta} + \frac{137}{36} C_A - \frac{23}{18} T_F n_f + \beta_0 \ln 2 - \frac{5}{12} C_A \pi^2 \right). \tag{59}$$

This coincides with the result on the unmeasured gluon jet function obtained in Ref. [18]. And the anomalous dimension of the gluon jet function is given by

$$\gamma_J = \frac{d}{d \ln \mu} \mathcal{J}_g = \frac{\alpha_s}{2\pi} \left(4C_A \ln \frac{\mu}{Q\delta} + \beta_0 \right). \quad (60)$$

VI. COLLINEAR QUARK DISTRIBUTION FUNCTION

When we consider the collinear part for the incoming partons near the threshold $x \sim 1$, there is another scale $Q(1-x)^{1/2}$, where x is the fraction of the longitudinal momentum of the parton with respect to the hadron. In order to deal with the scaling behavior of the incoming partons is to invoke the collinear distribution functions with the collinear momentum scaling as $p^\mu \sim Q(1, \eta, \eta^2)$ where $\eta = (1-x)^{1/2}$ [29]. The collinear distribution function scales from the collinear scale $Q\eta$ to the renormalization scale μ . Note that the small parameter η is independent of the small parameter λ in SCET. However, we can put $\eta \sim \lambda$ for definiteness.

Away from the threshold in which the beam jets are produced in the beam directions, the evolution of the initial-state particles from $Q\lambda$ to μ is described by the beam function. Near threshold, the collinear distribution function takes the role of the beam function away from the threshold. In a sense, the collinear distribution function is regarded as the beam function with the virtuality approaching zero.

The n -collinear distribution function from Eq. (9) can be written as

$$f_{q/N}(x, \mu) = \langle N | \bar{\chi}_n \frac{\bar{\not{n}}}{2} \delta(\bar{n} \cdot Px - \bar{n} \cdot \mathcal{P}) \chi_n | N \rangle. \quad (61)$$

The Feynman diagrams for the collinear distribution functions at one loop are shown in Fig. 7. Fig. 7 (a) is the virtual correction, Fig. 7 (b) and (c) are real gluon emissions, but Fig. 7 (c) is suppressed near threshold. The mirror images of Fig. 7 (a), (b) are omitted.

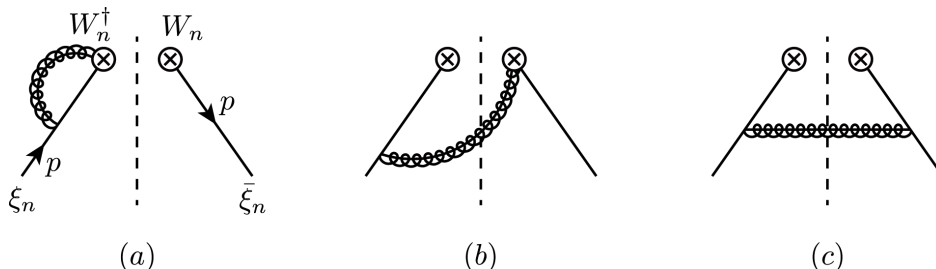


FIG. 7. Feynman diagrams for the n -collinear quark distribution function at one loop (a) virtual corrections, (b) and (c) real gluon emission. The mirror images of (a) and (b) are omitted.

The naive collinear contributions from Fig. 7 (a) and (b) are given as

$$\begin{aligned}
\tilde{M}_a &= 2ig^2 C_F \left(\frac{\mu^2 e^\gamma}{4\pi} \right)^\epsilon \delta(1-x) \int \frac{d^D l}{(2\pi)^D} \frac{\bar{n} \cdot (p-l)}{l^2 (l-p)^2 \bar{n} \cdot l} \\
&= \frac{\alpha_s C_F}{2\pi} \delta(1-x) \left(\frac{1}{\epsilon_{\text{UV}}} - \frac{1}{\epsilon_{\text{IR}}} \right) \left(\frac{1}{\epsilon_{\text{IR}}} + 1 + \ln \frac{\mu}{-Q} \right), \\
\tilde{M}_b &= -4\pi g^2 C_F \left(\frac{\mu^2 e^\gamma}{4\pi} \right)^\epsilon \int \frac{d^D l}{(2\pi)^D} \frac{\bar{n} \cdot (p-l)}{(l-p)^2 \bar{n} \cdot l} \delta(l^2) \delta\left(1-x - \frac{\bar{n} \cdot l}{\bar{n} \cdot p}\right) \\
&\rightarrow -\frac{\alpha_s C_F}{2\pi} \delta(1-x) \left(\frac{1}{\epsilon_{\text{UV}}} - \frac{1}{\epsilon_{\text{IR}}} \right) \left(\frac{1}{\epsilon_{\text{IR}}} + \ln \frac{\mu}{Q} \right), \tag{62}
\end{aligned}$$

where only the part proportional to $\delta(1-x)$ is extracted near threshold.

The zero-bin contributions are given as

$$\begin{aligned}
M_a^0 &= -2ig^2 C_F \left(\frac{\mu^2 e^\gamma}{4\pi} \right)^\epsilon \delta(1-x) \int \frac{d^D l}{(2\pi)^D} \frac{1}{l^2 \bar{n} \cdot l n \cdot l} \\
&= \frac{\alpha_s C_F}{2\pi} \delta(1-x) \left(\frac{1}{\epsilon_{\text{UV}}} - \frac{1}{\epsilon_{\text{IR}}} \right) \frac{1}{\epsilon_{\text{IR}}}, \\
M_b^0 &= 4\pi g^2 C_F \left(\frac{\mu^2 e^\gamma}{4\pi} \right)^\epsilon \int \frac{d^D l}{(2\pi)^D} \frac{1}{\bar{n} \cdot l n \cdot l} \delta(l^2) \delta\left(1-x - \frac{\bar{n} \cdot l}{\bar{n} \cdot p}\right) \\
&\rightarrow -\frac{\alpha_s C_F}{2\pi} \delta(1-x) \left(\frac{1}{\epsilon_{\text{UV}}} - \frac{1}{\epsilon_{\text{IR}}} \right) \left(\frac{1}{\epsilon_{\text{IR}}} + \ln \frac{\mu}{Q} \right) = M_b. \tag{63}
\end{aligned}$$

Note that the result of Eq. (21) is used in M_a^0 . This is because the one-loop correction of the collinear distribution function contains IR divergence, which is absorbed into the nonperturbative matrix element for the collinear distribution function. It is also true for the PDF. Therefore the choice of the prescription is important. The zero-bin subtraction in the collinear distribution function is closely related to the soft gluon emission in the beam direction. In order to disentangle the divergence in the collinear distribution function and the soft function, the prescription for the collinear distribution function should be the same as that employed in computing M^{beam} .

So far, only the terms proportional to $\delta(1-x)$ are extracted, since the remaining plus distribution functions are negligible near threshold. Since the dijet cross section is obtained by integrating over the fraction x , we will drop $\delta(1-x)$ from now on with the understanding that the integration over x is performed.

With the wave function renormalization at one loop

$$Z_f^{(1)} = -\frac{\alpha_s C_F}{4\pi} \left(\frac{1}{\epsilon_{\text{UV}}} - \frac{1}{\epsilon_{\text{IR}}} \right), \tag{64}$$

the collinear part at order α_s is given by

$$M_C = 2\text{Re}(\tilde{M}_a - M_a^0 + \tilde{M}_b - M_b^0) + Z_f^{(1)} = \frac{\alpha_s C_F}{2\pi} \left(\frac{1}{\epsilon_{\text{UV}}} - \frac{1}{\epsilon_{\text{IR}}} \right) \left(\frac{3}{2} + 2 \ln \frac{\mu}{Q} \right). \tag{65}$$

Therefore the anomalous dimension of the collinear distribution function is given by

$$\gamma_f = \frac{\alpha_s C_F}{2\pi} \left(3 + 4 \ln \frac{\mu}{Q} \right). \tag{66}$$

VII. EVOLUTION OF THE SCATTERING CROSS SECTION

The dijet cross section is schematically written as

$$\sigma = \sum_{IJ} H_{IJ}(\mu) S_{JI}(\mu) \otimes \mathcal{J}_g(\mu) \otimes \mathcal{J}_g(\mu) \otimes f_{q/N_1}(\xi_1, \mu) \otimes f_{\bar{q}/N_2}(\xi_2, \mu). \quad (67)$$

The cross section is a convolution of the hard function H_{IJ} , the soft function S_{JI} , the jet functions and the collinear distribution functions. Each function starts from appropriate scales μ_i and scales to the common scale μ . For the hard function, $\mu_H \sim Q$, for the soft function, $\mu_S \sim \beta Q$, for the jet function, $\mu_J \sim \delta Q$, and for the collinear distribution function, $\mu_C \sim \eta Q$. And the overall cross section is independent of the renormalization scale μ . The evolution of each component in the jet cross section can be obtained by solving the renormalization group equations.

A. The hard function

The hard function is given by $H_{IJ} = C_I C_J^*$, where C_I is the Wilson coefficient of O_I obtained by the matching between the full QCD and the SCET. The matching scale is of order $Q \sim \sqrt{S}$ near the threshold. The detailed form of the hard function at one loop for $2 \rightarrow 2$ partonic processes can be found in Ref. [16]. The relation between the bare and the renormalized hard functions is given by

$$\mathbf{H}_{\text{bare}} = \mathbf{Z}_H(\mu) \mathbf{H}(\mu) \mathbf{Z}_H^\dagger(\mu), \quad (68)$$

and the renormalization group equation for the hard function is given by

$$\frac{d}{d \ln \mu} \mathbf{H} = \mathbf{\Gamma}_H \mathbf{H} + \mathbf{H} \mathbf{\Gamma}_H^\dagger, \quad (69)$$

where the anomalous dimension matrix $\mathbf{\Gamma}_H$ is defined as

$$\mathbf{\Gamma}_H = -\mathbf{Z}_H^{-1} \frac{d}{d \ln \mu} \mathbf{Z}_H. \quad (70)$$

The anomalous dimension matrix $\mathbf{\Gamma}_H$ can be written as [11, 16]

$$\mathbf{\Gamma}_H = \frac{1}{2} \sum_{i=1}^4 \left[C_i \Gamma_c(\alpha_s) \ln \frac{-t}{\mu^2} - \frac{\alpha_s}{\pi} \gamma_i \right] \mathbf{1} + \Gamma_c(\alpha_s) \mathbf{M}, \quad (71)$$

where $\Gamma_c(\alpha_s)$ is the cusp anomalous dimension which can be expanded as [30]

$$\Gamma_c(\alpha_s) = \frac{\alpha_s}{4\pi} \Gamma_c^0 + \left(\frac{\alpha_s}{4\pi} \right)^2 \Gamma_c^1 + \dots, \quad (72)$$

with

$$\Gamma_c^0 = 4, \quad \Gamma_c^1 = \left(\frac{268}{9} - \frac{4}{3} \pi^2 \right) C_A - \frac{40n_f}{9}. \quad (73)$$

To next-to-leading logarithmic accuracy, the cusp anomalous dimension to two loops is needed. The Casimir invariants C_i are given by $C_q = C_F$, $C_g = C_A$, and γ_i are given by

$$\gamma_q = \frac{3}{2}C_F, \quad \gamma_g = \frac{\beta_0}{2}. \quad (74)$$

The matrix \mathbf{M} can be written as

$$\mathbf{M} = - \sum_{i < j} \mathbf{T}_i \cdot \mathbf{T}_j \left[L(s_{ij}) - L(t) \right], \quad (75)$$

where $s_{12} = s_{34} = (p_3 + p_4)^2 = s$, $s_{13} = s_{24} = (p_1 - p_3)^2 = t$, $s_{14} = s_{23} = (p_1 - p_4)^2 = u$, and $L(x)$ is given by

$$L(t) = \ln \frac{-t}{\mu^2}, \quad L(u) = \ln \frac{-u}{\mu^2}, \quad L(s) = \ln \frac{s}{\mu^2} - i\pi. \quad (76)$$

Specifically, for $q\bar{q} \rightarrow gg$, the first part of $\mathbf{\Gamma}_H$ in Eq. (71) is written as

$$\frac{\alpha_s}{2\pi} \left[-3C_F - \beta_0 + 2(C_F + C_A) \left(\ln \frac{n_{13}}{2} - 2 \ln \frac{\mu}{Q} \right) \right] \mathbf{1}, \quad (77)$$

and \mathbf{M} is given by

$$\begin{aligned} \frac{\alpha_s}{\pi} \mathbf{M} = & -\frac{\alpha_s C_F}{\pi} \ln \frac{n_{13}}{2} \mathbf{1} - i\pi \mathbf{T} \\ & + \frac{\alpha_s}{2\pi} \begin{pmatrix} 0 & 0 & 4 \ln \frac{n_{13}}{2} \\ 0 & -2C_A \ln \frac{n_{13}}{2} & 4 \ln \frac{n_{14}}{2} \\ -\ln \frac{n_{14}}{2} & -\ln \frac{n_{13}}{2} & -2C_A \ln \frac{n_{13}}{2} \end{pmatrix}, \end{aligned} \quad (78)$$

where \mathbf{T} is given by

$$\mathbf{T} = \frac{\alpha_s}{2\pi} \begin{pmatrix} 2C_F & 0 & 0 \\ 0 & 2C_F & 0 \\ 1 & 1 & 2(C_F + C_A) \end{pmatrix}. \quad (79)$$

B. The soft function

The soft function is renormalized like the hard function as

$$\mathbf{S}_{\text{bare}} = \mathbf{Z}_S^\dagger(\mu) \mathbf{S}(\mu) \mathbf{Z}_S(\mu), \quad (80)$$

and the renormalization group equation is given as

$$\frac{d}{d \ln \mu} \mathbf{S} = \mathbf{S} \mathbf{\Gamma}_S + \mathbf{\Gamma}_S^\dagger \mathbf{S}, \quad (81)$$

where $\mathbf{\Gamma}_S$ is defined as

$$\mathbf{\Gamma}_S = - \left(\frac{d}{d \ln \mu} \mathbf{Z}_S \right) \mathbf{Z}_S^{-1}. \quad (82)$$

The soft contributions at one loop are given as

$$\begin{aligned}
\mathcal{M}_{12} &= -\frac{\alpha_s \pi^2}{2\pi \cdot 6}, \\
\mathcal{M}_{ij} &= \frac{\alpha_s}{2\pi} \left[2 \ln \frac{2\delta}{n_{ij}} \ln \frac{\mu}{2\beta Q} - \ln^2 \delta - \text{Li}_2 \left(1 - \frac{2}{n_{ij}} \right) - \frac{\pi^2}{6} \right], \\
\mathcal{M}_{34} &= \frac{\alpha_s}{2\pi} \left[4 \ln \delta \ln \frac{\mu}{2\beta Q} - 2 \ln^2 \delta - \frac{\pi^2}{6} \right].
\end{aligned} \tag{83}$$

And the functions $(\alpha_s/2\pi)U_{ij}^S \equiv d\mathcal{M}_{ij}/d\ln\mu$ are given by

$$U_{12}^S = 0, \quad U_{ij}^S = 2 \ln \frac{2\delta}{n_{ij}}, \quad U_{34}^S = 4 \ln \delta. \tag{84}$$

The following combination from the soft contributions is given by

$$\begin{aligned}
& - \sum_{i<j} \mathbf{T}_i \cdot \mathbf{T}_j U_{ij}^S \\
&= \begin{pmatrix} \left(C_F - \frac{C_A}{2}\right)U_{12} + \frac{C_A}{2}(U_{34} + 2U_{13}) & 0 & 2(U_{13} - U_{14}) \\ 0 & \left(C_F - \frac{C_A}{2}\right)U_{12} + \frac{C_A}{2}(U_{34} + 2U_{14}) & 2(U_{14} - U_{13}) \\ \frac{1}{4}(U_{12} + U_{34} - 2U_{14}) & \frac{1}{4}(U_{12} + U_{34} - 2U_{13}) & C_F U_{12} + C_A U_{34} \end{pmatrix} \\
&= 4C_A \ln \delta \mathbf{1} + \begin{pmatrix} -2C_A \ln \frac{n_{13}}{2} & 0 & 4 \ln \frac{n_{14}}{n_{13}} \\ 0 & -2C_A \ln \frac{n_{14}}{2} & 4 \ln \frac{n_{13}}{n_{14}} \\ \ln \frac{n_{14}}{2} & \ln \frac{n_{13}}{2} & 0 \end{pmatrix},
\end{aligned} \tag{85}$$

where the fact that $U_{13} = U_{24}$, $U_{14} = U_{23}$ is used. And the anomalous dimension of the soft function is given as

$$\mathbf{\Gamma}_S = -\frac{\alpha_s}{2\pi} \sum_{i<j} \mathbf{T}_i \cdot \mathbf{T}_j U_{ij}^S + i\pi \mathbf{T}, \tag{86}$$

where we have inserted \mathbf{T} to keep the consistency of the anomalous dimensions, and it does not affect Eq. (87) below at one loop since $\mathbf{S}_0 \mathbf{T} = \mathbf{T}^\dagger \mathbf{S}_0$.

C. Cancellation of the anomalous dimensions

The dijet cross section should be independent of the renormalization scale, which means that the sum of the anomalous dimensions of the factorized parts should be zero. At next-to-leading order, the derivative of the dijet cross section in Eq. (67) with respect to $\ln\mu$ yields

$$\begin{aligned}
\frac{d\sigma}{d\ln\mu} &= \left[\text{tr } \mathbf{H}_0 \mathbf{S}_0 \left(\mathbf{\Gamma}_H + \mathbf{\Gamma}_S + (\gamma_J + \gamma_f) \mathbf{1} \right) + \text{tr } \mathbf{S}_0 \mathbf{H}_0 \left(\mathbf{\Gamma}_H^\dagger + \mathbf{\Gamma}_S^\dagger + (\gamma_J + \gamma_f) \mathbf{1} \right) \right] \\
&\quad \otimes \mathcal{J}_{g,0} \otimes \mathcal{J}_{g,0} \otimes \left(f_{q/N_1,0} \otimes f_{\bar{q}/N_2,0} + (q \leftrightarrow \bar{q}) \right),
\end{aligned} \tag{87}$$

where the quantities with the subscript 0 are the tree-level quantities. The anomalous dimensions of the gluon jet function and the collinear distribution function are given by

$$\gamma_J = \frac{\alpha_s}{2\pi} \left(4C_A \ln \frac{\mu}{Q\delta} + \beta_0 \right), \quad \gamma_f = \frac{\alpha_s C_F}{2\pi} \left(3 + 4 \ln \frac{\mu}{Q} \right). \quad (88)$$

From Eqs. (71), (86), the sum of the anomalous dimension matrices $\mathbf{\Gamma}_H + \mathbf{\Gamma}_S$ becomes diagonal and is given by

$$\mathbf{\Gamma}_H + \mathbf{\Gamma}_S = \frac{\alpha_s}{2\pi} \mathbf{1} \left[-3C_F - \beta_0 - 4(C_F + C_A) \ln \frac{\mu}{Q} + 4C_A \ln \delta \right] = -(\gamma_J + \gamma_f) \mathbf{1}, \quad (89)$$

which satisfies

$$\mathbf{\Gamma}_H + \mathbf{\Gamma}_S + (\gamma_J + \gamma_f) \mathbf{1} = 0. \quad (90)$$

Therefore the dijet cross section is independent of the renormalization scale μ . The evolution of the hard, jet, collinear distribution and soft functions can be performed in a standard way [11, 16, 31].

VIII. CONCLUSION

The factorization theorems for various physical observables ranging from the jet cross sections to more differential quantities such as the jet substructure are crucial in theoretical prediction. Once the factorization theorems are provided, each factorized part or its evolution can be computed using perturbation theory. When there are hierarchies of scales, as often happens in high-energy scattering, large logarithms of the ratio of disparate scales appear and they can be resummed using the renormalization group equation. However, in order to resum the large logarithms, we have to ensure that the divergences are purely of the UV origin. Therefore the proof of the IR finiteness in each factorized part is vital in proving factorization theorems.

In this paper, we have considered the basic quantity, which is the dijet cross section in hadron-hadron scattering. We expect that the more differential the physical quantities we probe, the more complicated becomes the verification of the IR finiteness. And this is just the starting point in that direction. Though the dijet cross section looks simple, it contains a lot of interesting physics as we delved deeper into the divergence structure in this paper.

As far as the divergence structure is concerned, the existence of the beam particles is important in constructing a dijet event. In e^+e^- annihilation, there are no initial hadrons and all the outgoing particles can form jets. That is, we can apply the jet algorithm to all the outgoing particles. For example, in order to form a dijet event, we see if two particles are adjacent to each other, they form a jet. If a soft particle is emitted outside the jet, its energy should be small enough to be excluded as a jet by a jet veto. However, in hadron-hadron scattering, if soft particles above the jet veto outside the jets are emitted in the beam directions, this event is also counted as a dijet event, and this case is missing with the jet algorithm alone. Without this contribution, the soft function with the jet algorithm still remains IR divergent. Only after this additional contribution is added, the IR finiteness

of the factorization theorem is completed. Therefore there is definite distinction between e^+e^- annihilation and hadron-hadron scattering when we try to distinguish the origin of the divergence.

We have also computed the anomalous dimensions of the hard, collinear and soft parts. The anomalous dimensions of the collinear quark distribution functions and the gluon jet functions are diagonal in color space, and those of the hard and soft functions are nontrivial matrices. On the other hand, the jet algorithm affects the color-diagonal gluon jet function and the color non-diagonal soft function. In order for the sum of the anomalous dimensions to cancel, the dependence of the jet algorithm on the soft function should reside in the diagonal part only to be cancelled by the diagonal gluon jet function which depends on the jet algorithm. And the off-diagonal terms in the soft function should be cancelled by those in the hard function. All these intertwined structure of the anomalous dimensions are explicitly shown in our example of the process $q\bar{q} \rightarrow gg$.

As already mentioned, the detailed analysis of the IR divergence should be applied to other processes. For example, the IR finiteness should be verified in the dijet cross section away from threshold, in which there are beam jets. We can also consider the jet cross section with the resummation for small R . In this case, an additional mode called the soft-collinear mode [19] is considered and we expect that the IR divergence structure is richer and more complicated. The analysis on more differential quantities, such as thrust or invariant jet mass distribution [32] is also required because there may exist delicate structure of the phase space, which invokes additional IR divergences to consider. These are the topics to be pursued in the near future.

ACKNOWLEDGMENTS

The authors are supported by Basic Science Research Program through the National Research Foundation of Korea (NRF) funded by the Ministry of Education(Grant No. NRF-2014R1A1A2058142).

Appendix A: Computation of the soft part M_{ij}^{jet}

The soft part M_{ij}^{jet} is given by

$$M_{ij}^{\text{jet}} = g^2 \left(\frac{\mu^2 e^\gamma}{4\pi} \right)^\epsilon \int \frac{d^D l}{(2\pi)^D} \frac{n_i \cdot n_j}{n_i \cdot l n_j \cdot l} 2\pi \delta(l^2) \Theta(l_0 > \beta Q) \Theta_J. \quad (\text{A1})$$

In order to compute the contributions systematically, let us classify it in two parts. The first is written as M_{ij}^j , where the subscripts i and j refer to the indices appearing in the denominator in Eq. (A1), and the superscript denotes the jet direction. For example, M_{13}^3 means that the denominator is given by $n_1 \cdot l n_3 \cdot l$ and we consider the jet algorithm for the n_3 jet. The second one is written as M_{ij}^k , where the subscripts mean the same denominator, but the superscript k refers to the n_k jet directions with k being neither i , nor j . For example,

M_{13}^4 means the beam-jet contribution with the denominator $n_1 \cdot l n_3 \cdot l$ and the jet algorithm for the n_4 jet.

1. M_{ij}^j

We can choose the lightcone vector in the j direction as $n_j^\mu = (1, 0, 0, 1)$, and $n_i^\mu = (1, \sin \rho, 0, \cos \rho)$, which is obtained by rotating the spatial part of n_j^μ by the angle ρ around the y axis. We write l^μ in the n_j basis as

$$l^\mu = \frac{n_j^\mu}{2} l_- + \frac{\bar{n}_j^\mu}{2} l_+ + l_\perp^\mu, \quad (\text{A2})$$

where $l_\perp^\mu = (0, l_{\perp 1}, l_{\perp 2}, 0)$ is the perpendicular momentum with respect to n_j and \bar{n}_j such that $n_j \cdot l_\perp = \bar{n}_j \cdot l_\perp = 0$, but $n_i \cdot l_\perp$ need not be zero. Then $n_i \cdot l$ is given by

$$n_i \cdot l = \frac{1 - \cos \rho}{2} l_- + \frac{1 + \cos \rho}{2} l_+ - l_{\perp 1} \sin \rho. \quad (\text{A3})$$

Since the integrand is independent of $l_{\perp 2}$, we write the integration measure as

$$d^D l = \frac{1}{2} dl_- dl_+ dl_{\perp 1} d^{D-3} l_{\perp 2}, \quad (\text{A4})$$

and $d^{D-3} l_{\perp 2} = d|l_{\perp 2}| |l_{\perp 2}|^{D-4} d\Omega_{D-3}$. After integrating over $d\Omega_{D-3}$ and using $l_{\perp 1} = |\mathbf{l}_\perp| \cos \phi$, $l_{\perp 2} = |\mathbf{l}_\perp| \sin \phi$, the integration measure is written as

$$d^D l = \frac{\pi^{1/2-\epsilon}}{2\Gamma(\frac{1}{2}-\epsilon)} dl_- dl_+ d\mathbf{l}_\perp^2 (\mathbf{l}_\perp^2)^{-\epsilon} d\phi \sin^{-2\epsilon} \phi \Theta(0 < \phi < \pi). \quad (\text{A5})$$

Then M_{ij}^j can be written as

$$\begin{aligned} M_{ij}^j &= \frac{\alpha_s}{2\pi} \frac{(\mu^2 e^\gamma)^\epsilon}{\sqrt{\pi} \Gamma(\frac{1}{2}-\epsilon)} \frac{n_{ij}}{2} \int dl_+ dl_- l_+^{-1-\epsilon} l_-^{-\epsilon} \Theta(l_- + l_+ > 2\beta Q) \Theta(l_+ < l_- \delta^2) \\ &\times \int_0^\pi d\phi \frac{2 \sin^{-2\epsilon} \phi}{n_{ij} l_- + \bar{n}_{ij} l_+ - 2\sqrt{l_+ l_-} \sin \rho \cos \phi}, \end{aligned} \quad (\text{A6})$$

where $n_{ij} = n_i \cdot n_j$ and $\bar{n}_{ij} = n_i \cdot \bar{n}_j$. We now change the variable as $v = \sqrt{l_+/l_-}$, and the theta functions become $\Theta(l_- > \alpha)$ with $\alpha = 2\beta Q/(1+v^2)$ and $\Theta(0 < v < \delta)$. Note that the integration over v corresponds to the angular integral in the $l_- l_+$ phase space. With the change of the variables, M_{ij}^j is given by

$$M_{ij}^j = \frac{\alpha_s}{2\pi} \frac{(\mu^2 e^\gamma)^\epsilon n_{ij}}{\sqrt{\pi} \Gamma(\frac{1}{2}-\epsilon)} \int_0^\delta dv v^{-1-2\epsilon} \int_0^\pi d\phi \frac{2 \sin^{-2\epsilon} \phi}{n_{ij} + v^2 \bar{n}_{ij} - 2v \sin \rho \cos \phi} \int_\alpha^\infty dl_- l_-^{-1-2\epsilon}. \quad (\text{A7})$$

In order to extract the UV and IR divergences correctly, the l_- -integral is computed as

$$\mu^{2\epsilon} \int_\alpha^\infty l_-^{-1-2\epsilon} = \mu^{2\epsilon} \left(\int_0^\infty dl_- l_-^{-1-2\epsilon} - \int_0^\alpha dl_- l_-^{-1-2\epsilon} \right) = \frac{1}{2} \left(\frac{1}{\epsilon_{\text{UV}}} - \frac{1}{\epsilon_{\text{IR}}} \right) + \frac{1}{2\epsilon_{\text{IR}}} \left(\frac{\mu}{\alpha} \right)^{2\epsilon}. \quad (\text{A8})$$

After integrating over l_- , M_{ij}^j can be rewritten as

$$\begin{aligned}
M_{ij}^j = & \frac{\alpha_s}{2\pi} \frac{(\mu^2 e^\gamma)^\epsilon}{\sqrt{\pi} \Gamma(\frac{1}{2} - \epsilon)} \left\{ \left[\frac{1}{\epsilon_{\text{UV}}} - \frac{1}{\epsilon_{\text{IR}}} + \frac{1}{\epsilon_{\text{IR}}} \left(\frac{\mu}{2\beta Q} \right)^{2\epsilon} \right] \int_0^\delta dv v^{-1-2\epsilon} \int_0^\pi d\phi \sin^{-2\epsilon} \phi \right. \\
& + \frac{n_{ij}}{2} \left(\frac{1}{\epsilon_{\text{UV}}} - \frac{1}{\epsilon_{\text{IR}}} \right) \int_0^\delta dv v^{-1-2\epsilon} \int_0^\pi d\phi \left(\frac{2 \sin^{-2\epsilon} \phi}{n_{ij} + v^2 \bar{n}_{ij} - 2v \sin \rho \cos \phi} - \frac{2 \sin^{-2\epsilon} \phi}{n_{ij}} \right) \\
& \left. + \frac{n_{ij}}{2} \frac{1}{\epsilon_{\text{IR}}} \left(\frac{\mu}{2\beta Q} \right)^{2\epsilon} \int_0^\delta dv v^{-1-2\epsilon} \int_0^\pi d\phi \left(\frac{2(1+v^2)^{2\epsilon} \sin^{-2\epsilon} \phi}{n_{ij} + v^2 \bar{n}_{ij} - 2v \sin \rho \cos \phi} - \frac{2 \sin^{-2\epsilon} \phi}{n_{ij}} \right) \right\}. \quad (\text{A9})
\end{aligned}$$

The integrands in the last two terms are finite as $v \rightarrow 0$, and they can be expanded to order v to obtain the final result, to order δ^2 , as

$$\begin{aligned}
M_{ij}^j = & \frac{\alpha_s}{2\pi} \left(-\frac{1}{2\epsilon_{\text{UV}}\epsilon_{\text{IR}}} - \frac{1}{\epsilon_{\text{IR}}} \ln \frac{\mu}{2\beta Q} + \frac{1}{\epsilon_{\text{UV}}} \ln \delta - \ln^2 \frac{\mu}{2\beta Q \delta} + \frac{\pi^2}{24} \right) \\
& + \frac{\alpha_s}{2\pi} \delta^2 \left[1 + \frac{2 - n_{ij}}{n_{ij}} \left(\frac{3}{2} + \frac{1}{2\epsilon_{\text{UV}}} + \ln \frac{\mu}{2\delta\beta Q} \right) \right], \quad (\text{A10})
\end{aligned}$$

where the relations $n_{ij}\bar{n}_{ij} = \sin^2 \rho$ and $n_{ij} + \bar{n}_{ij} = 2$ are used.

2. M_{ij}^k

In this calculation, we express $n_i \cdot l$ and $n_j \cdot l$ in the denominator in the basis of n_k , \bar{n}_k , and their perpendicular directions. We can choose these lightcone vectors as

$$n_k = (1, 0, 0, 1), \quad n_i = (1, \sin \theta_i, 0, \cos \theta_i), \quad n_j = (1, \sin \theta_j, 0, \cos \theta_j), \quad (\text{A11})$$

where θ_i and θ_j are the angles rotated with respect to the y axis and the scattering occurs in the xz plane. Note that $\theta_i, \theta_j \gg \delta$ since the n_i and n_j are away from the jet direction n_k .

Then M_{ij}^k can be written as

$$\begin{aligned}
M_{ij}^k = & \frac{\alpha_s}{2\pi} \frac{(\mu^2 e^\gamma)^\epsilon}{\sqrt{\pi} \Gamma(\frac{1}{2} - \epsilon)} \frac{n_{ij}}{2} \int dl_- dl_+ (l_- l_+)^{-\epsilon} \Theta(l_- + l_+ > 2\beta Q) \Theta(l_+ < \delta^2 l_-) \int_0^\pi d\phi \\
& \times \frac{4 \sin^{-2\epsilon} \phi}{(n_{ik} l_- + \bar{n}_{ik} l_+ - 2\sqrt{l_- l_+} \sin \theta_i \cos \phi)(n_{jk} l_- + \bar{n}_{jk} l_+ - 2\sqrt{l_- l_+} \sin \theta_j \cos \phi)} \\
= & \frac{\alpha_s}{2\pi} \frac{(\mu^2 e^\gamma)^\epsilon}{\sqrt{\pi} \Gamma(\frac{1}{2} - \epsilon)} n_{ij} \int_0^\delta dv v^{1-2\epsilon} \int_\alpha^\infty dl_- l_-^{-1-2\epsilon} \\
& \times \int_0^\pi d\phi \frac{4 \sin^{-2\epsilon} \phi}{(n_{ik} + v^2 \bar{n}_{ik} - 2v \sin \theta_i \cos \phi)(n_{jk} + v^2 \bar{n}_{jk} - 2v \sin \theta_j \cos \phi)}, \quad (\text{A12})
\end{aligned}$$

where the last line is obtained by changing the variable $l_+ = v^2 l_-$.

Integrating over l_- yields an UV divergence, and the remaining integral over v and ϕ is finite. We expand the integrand in powers of v , and the final result to order δ^2 is given as

$$M_{ij}^k = \frac{\alpha_s}{2\pi} \delta^2 \frac{n_{ij}}{n_{ik} n_{jk}} \left(1 + \frac{1}{\epsilon_{\text{UV}}} + 2 \ln \frac{\mu}{2\delta\beta Q} \right). \quad (\text{A13})$$

Appendix B: Derivation of the soft contribution in the beam direction

The soft contribution in the beam direction can be obtained either from the beam-beam contribution or from the beam-jet contribution, and the result is the same. Note that the soft contribution in the beam direction should include only the IR divergence since there is a collinear divergence involved. Therefore IR or mixed divergences are included. We present here how the beam contribution M^{beam} can be computed from the beam-beam and the beam-jet contributions respectively.

1. The beam-beam contribution

The contribution from the emission of soft gluons in the beam direction can be obtained in three steps. First, the contribution in the beam direction with $l_0 > \beta Q$ consists of only the collinear IR divergence, which is to be extracted. Second, the contribution from the entire phase space with no constraint from the jet algorithm is given by the negative of the virtual correction, $-M_{ij}^V$, and it only contains the divergence without any finite part. Third, when the contribution from the jet veto is subtracted from the contribution over the whole phase space, it gives twice the beam contribution.

If there exists only the UV divergence from the region $l_{\pm} \rightarrow \infty$, this method fails. But fortunately, when the contribution from the whole phase space is computed using Eq. (21), there is no UV divergence alone, but IR or mixed divergence. In this sense, the approach in Eq. (19) is not appropriate in computing M^{beam} from this approach. Another point is that, when the divergent part is extracted, the finite part accompanied by the divergence should be included. For example, if there is a term $1/\epsilon_{\text{IR}}$, the term $2 \ln(\mu/2\beta Q)$ should be accompanied. Otherwise, the derivations of the anomalous dimensions from the counter terms and from the μ -dependent part become inconsistent. And if there is $1/\epsilon_{\text{IR}}^2$, a factor $1/\Gamma(1-\epsilon)$ is attached, hence the term $-\pi^2/12$ is to be included.

From the argument above, the divergent part from M_{12}^{veto} is given by

$$M_{12}^{d,\text{veto}} = \frac{\alpha_s}{2\pi} \left(\frac{1}{\epsilon_{\text{IR}}^2} + \frac{1}{\epsilon_{\text{IR}}} \left(2 \ln \frac{\mu}{2\beta Q} - \ln \frac{n_{12}}{2} \right) + 2 \ln^2 \frac{\mu}{2\beta Q} - 2 \ln \frac{\mu}{2\beta Q} \ln \frac{n_{12}}{2} - \frac{\pi^2}{12} \right). \quad (\text{B1})$$

All the divergent parts satisfy the relation $M_{12}^{d,\text{veto}} + 2M_0^{\text{beam}} = -M_V$, from which the soft contribution in the beam direction, still with the UV divergence, is given as

$$\begin{aligned} M_0^{\text{beam}} &= -\frac{1}{2}(M_V + M_{12}^{d,\text{veto}}) \\ &= \frac{\alpha_s}{2\pi} \left[-\frac{1}{2\epsilon_{\text{UV}}\epsilon_{\text{IR}}} - \frac{1}{\epsilon_{\text{IR}}} \ln \frac{\mu}{2\beta Q} - \ln^2 \frac{\mu}{2\beta Q} + \frac{\pi^2}{24} + \left(\frac{1}{2\epsilon_{\text{UV}}} + \ln \frac{\mu}{2\beta Q} \right) \ln \frac{n_{12}}{2} \right]. \end{aligned} \quad (\text{B2})$$

The last term is associated with the UV divergence. It does not belong to the collinear divergence, hence discarded to obtain M^{beam} . Finally, the soft contribution in the beam direction is given by

$$M^{\text{beam}} = \frac{\alpha_s}{2\pi} \left(-\frac{1}{2\epsilon_{\text{UV}}\epsilon_{\text{IR}}} - \frac{1}{\epsilon_{\text{IR}}} \ln \frac{\mu}{2\beta Q} - \ln^2 \frac{\mu}{2\beta Q} + \frac{\pi^2}{24} \right). \quad (\text{B3})$$

2. The beam-jet contribution

We can also compute M^{beam} in the beam-jet contribution. First, extracting the divergent part, $M_{ij}^{d,\text{veto}}$ is given by

$$M_{ij}^{d,\text{veto}} = \frac{\alpha_s}{2\pi} \left[\frac{1}{\epsilon_{\text{IR}}^2} + \frac{1}{\epsilon_{\text{IR}}} \left(2 \ln \frac{\mu}{2\beta Q} - \ln \frac{n_{ij}}{2} \right) + 2 \ln^2 \frac{\mu}{2\beta Q} - 2 \ln \frac{\mu}{2\beta Q} \ln \frac{n_{ij}}{2} - \frac{\pi^2}{12} \right]. \quad (\text{B4})$$

Also, dropping the UV divergent part and the finite term $-\ln^2 \delta$ in M_{ij}^{jet} , the relevant IR divergent term and those associated with it are given as

$$M_{ij}^{d,\text{jet}} = \frac{\alpha_s}{2\pi} \left(-\frac{1}{2\epsilon_{\text{UV}}\epsilon_{\text{IR}}} - \frac{1}{\epsilon_{\text{IR}}} \ln \frac{\mu}{2\beta Q} - \ln^2 \frac{\mu}{2\beta Q} + \frac{\pi^2}{24} \right). \quad (\text{B5})$$

From the relation $M_{ij}^{d,\text{veto}} + M_0^{\text{beam}} + M_{ij}^{d,\text{jet}} = -M_V$, we obtain

$$\begin{aligned} M_0^{\text{beam}} &= -(M_V + M_{ij}^{d,\text{veto}} + M_{ij}^{d,\text{jet}}) \\ &= \frac{\alpha_s}{2\pi} \left[-\frac{1}{2\epsilon_{\text{UV}}\epsilon_{\text{IR}}} - \frac{1}{\epsilon_{\text{IR}}} \ln \frac{\mu}{2\beta Q} - \ln^2 \frac{\mu}{2\beta Q} + \frac{\pi^2}{24} + \left(\frac{1}{\epsilon_{\text{UV}}} + 2 \ln \frac{\mu}{2\beta Q} \right) \ln \frac{n_{ij}}{2} \right]. \end{aligned} \quad (\text{B6})$$

The last term is of the UV origin, which should be discarded to obtain M^{beam} as

$$M^{\text{beam}} = \frac{\alpha_s}{2\pi} \left(-\frac{1}{2\epsilon_{\text{UV}}\epsilon_{\text{IR}}} - \frac{1}{\epsilon_{\text{IR}}} \ln \frac{\mu}{2\beta Q} - \ln^2 \frac{\mu}{2\beta Q} + \frac{\pi^2}{24} \right). \quad (\text{B7})$$

This result is the same as Eq. (B3) obtained in the beam-beam contribution.

-
- [1] C. W. Bauer, S. Fleming and M. E. Luke, Summing Sudakov logarithms in $B \rightarrow X_s \gamma$ in effective field theory, Phys. Rev. D **63**, 014006 (2000).
 - [2] C. W. Bauer, S. Fleming, D. Pirjol and I. W. Stewart, An Effective field theory for collinear and soft gluons: Heavy to light decays, Phys. Rev. D **63**, 114020 (2001).
 - [3] C. W. Bauer, D. Pirjol and I. W. Stewart, Soft collinear factorization in effective field theory, Phys. Rev. D **65**, 054022 (2002).
 - [4] I. W. Stewart, F. J. Tackmann, J. R. Walsh and S. Zuberi, Jet p_T resummation in Higgs production at NNLL'+NNLO, Phys. Rev. D **89**, no. 5, 054001 (2014).
 - [5] M. Dasgupta, A. Fregoso, S. Marzani and G. P. Salam, Towards an understanding of jet substructure, JHEP **1309**, 029 (2013).
 - [6] T. Kinoshita, Mass singularities of Feynman amplitudes, J. Math. Phys. **3**, 650 (1962).
 - [7] T. D. Lee and M. Nauenberg, Degenerate Systems and Mass Singularities, Phys. Rev. **133**, B1549 (1964).

- [8] J. Chay, C. Kim and I. Kim, Factorization of the dijet cross section in electron-positron annihilation with jet algorithms, *Phys. Rev. D* **92**, no. 3, 034012 (2015).
- [9] J. Chay, C. Kim and I. Kim, Analysis of exclusive k_T jet algorithms in electron-positron annihilation, *Phys. Rev. D* **92**, no. 7, 074019 (2015).
- [10] G. P. Salam, Towards Jetography, *Eur. Phys. J. C* **67**, 637 (2010).
- [11] A. Hornig, Y. Makris and T. Mehen, Jet Shapes in Dijet Events at the LHC in SCET, *JHEP* **1604**, 097 (2016).
- [12] I. W. Stewart, F. J. Tackmann and W. J. Waalewijn, Factorization at the LHC: From PDFs to Initial State Jets, *Phys. Rev. D* **81**, 094035 (2010).
- [13] T. T. Jouttenus, Jet Function with a Jet Algorithm in SCET, *Phys. Rev. D* **81**, 094017 (2010).
- [14] W. M. Y. Cheung, M. Luke and S. Zuberi, Phase Space and Jet Definitions in SCET, *Phys. Rev. D* **80**, 114021 (2009).
- [15] R. K. Ellis and J. C. Sexton, QCD Radiative Corrections to Parton Parton Scattering, *Nucl. Phys. B* **269**, 445 (1986).
- [16] R. Kelley and M. D. Schwartz, 1-loop matching and NNLL resummation for all partonic 2 to 2 processes in QCD, *Phys. Rev. D* **83**, 045022 (2011).
- [17] J. y. Chiu, A. Fuhrer, R. Kelley and A. V. Manohar, Factorization Structure of Gauge Theory Amplitudes and Application to Hard Scattering Processes at the LHC, *Phys. Rev. D* **80**, 094013 (2009).
- [18] S. D. Ellis, C. K. Vermilion, J. R. Walsh, A. Hornig and C. Lee, Jet Shapes and Jet Algorithms in SCET, *JHEP* **1011**, 101 (2010).
- [19] Y. T. Chien, A. Hornig and C. Lee, Soft-collinear mode for jet cross sections in soft collinear effective theory, *Phys. Rev. D* **93**, no. 1, 014033 (2016).
- [20] M. Dasgupta and G. P. Salam, Resummation of nonglobal QCD observables, *Phys. Lett. B* **512**, 323 (2001).
- [21] A. Idilbi and T. Mehen, On the equivalence of soft and zero-bin subtractions, *Phys. Rev. D* **75**, 114017 (2007).
- [22] A. Hornig, C. Lee and G. Ovanessian, Infrared Safety in Factorized Hard Scattering Cross-Sections, *Phys. Lett. B* **677**, 272 (2009).
- [23] J. Chay, C. Kim, Y. G. Kim and J. P. Lee, Soft Wilson lines in soft-collinear effective theory, *Phys. Rev. D* **71**, 056001 (2005).

- [24] S. Catani and M. H. Seymour, The Dipole formalism for the calculation of QCD jet cross-sections at next-to-leading order, *Phys. Lett. B* **378**, 287 (1996).
- [25] S. Catani and M. H. Seymour, A General algorithm for calculating jet cross-sections in NLO QCD, *Nucl. Phys. B* **485**, 291 (1997), Erratum: [*Nucl. Phys. B* **510**, 503 (1998)].
- [26] T. Becher and M. D. Schwartz, Direct photon production with effective field theory, *JHEP* **1002**, 040 (2010).
- [27] T. Becher and G. Bell, The gluon jet function at two-loop order, *Phys. Lett. B* **695**, 252 (2011).
- [28] A. V. Manohar and I. W. Stewart, The Zero-Bin and Mode Factorization in Quantum Field Theory, *Phys. Rev. D* **76**, 074002 (2007).
- [29] J. Chay and C. Kim, Proper factorization theorems in high-energy scattering near the endpoint, *JHEP* **1309**, 126 (2013).
- [30] G. P. Korchemsky and A. V. Radyushkin, Renormalization of the Wilson Loops Beyond the Leading Order, *Nucl. Phys. B* **283**, 342 (1987).
- [31] N. Kidonakis, G. Oderda and G. F. Sterman, Evolution of color exchange in QCD hard scattering, *Nucl. Phys. B* **531**, 365 (1998).
- [32] C. W. Bauer, F. J. Tackmann, J. R. Walsh and S. Zuberi, Factorization and Resummation for Dijet Invariant Mass Spectra, *Phys. Rev. D* **85**, 074006 (2012).